

Asset Pricing with the Awareness of New Risks

May 21, 2025

ABSTRACT

Recessions cause substantial but delayed drops in output, followed by recoveries with abnormally high growth. We propose a new theory where the awareness of new risks negatively impacts growth, leading to recessions of varying duration and severity. Our model shows that risk premia and return volatilities exhibit a hump-shaped pattern at the onset of recessions, not rising immediately, unlike in most non-expected utility models (Ai and Bansal, 2018). These results align with empirical patterns of output, risk premia, and volatilities observed during recessions. Hence, our model explains a stronger link between fundamentals and asset prices observed during recessions and recoveries.

JEL Classification: G12, E32, E44, G01.

Keywords: hump-shaped risk premia, hump-shaped volatilities, *U*-shaped output, new priced risk during crises, crisis heterogeneity

Preceding a crisis, there is often a heightened awareness of new risks. Take, for instance, the early days of 2020 when news emerged about a novel virus. Initially, this news did not trigger a crisis, as it remained uncertain whether the virus could be contained or if it would evolve into a full-fledged pandemic. While people were already aware of the presence of this new risk (the COVID-19 virus), there was still a lot of uncertainty about what the consequences would be. The COVID-19 pandemic serves as a vivid illustration of how an entirely new risk can disrupt the world, yet this awareness of new risks is not unique to that particular episode. In Figure 1, we present Google search trends for “*subprime*,” “*housing crisis*,” and “*mortgage crisis*,” key terms associated with the Global Financial Crisis. This figure reveals that even prior to the onset of the recession, there was a notable surge in interest surrounding topics related to what later became recognized as pivotal factors contributing to the crisis.

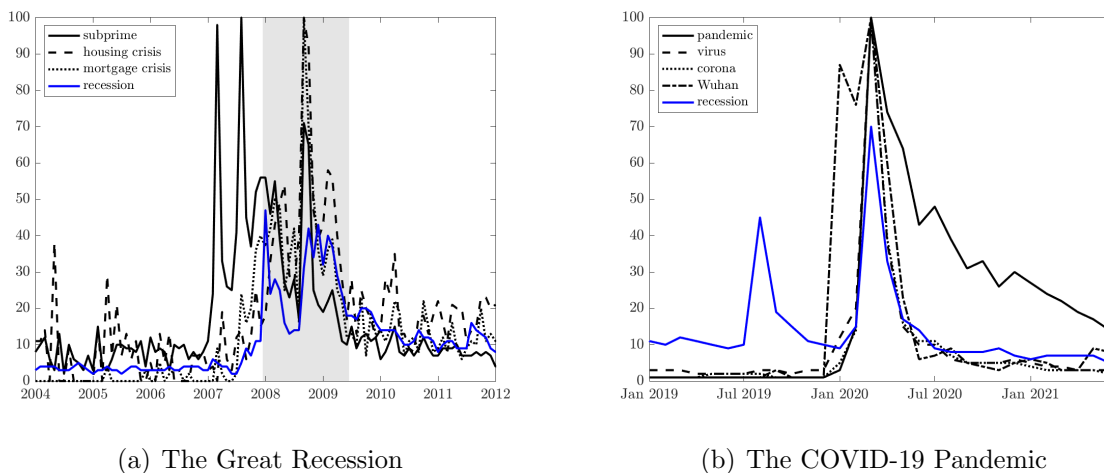


Figure 1. Awareness of New Risks. This figure displays the Google Trend word count for crisis terms related to two distinct events: the Global Financial Crisis (a) and the Covid-19 Pandemic recession (b). Data comes from Google Trends, which starts in 2004. Numbers represent search interest relative to the highest point on the chart for the given region and time. A value of 100 is the peak popularity for the term.

Asset prices are forward-looking indicators that reflect investors’ expectations about future economic activity. Typically, one might expect the emergence of new risks and the anticipation of an economic slowdown to be immediately reflected in asset prices, leading

to an immediate decline upon the discovery of a new risk. However, data shows that asset prices do not fall immediately. Instead, recessions materialize when bad news about the new risk unfolds, and expectations worsen progressively as a series of adverse shocks occur. This deterioration in both actual shocks and investors' expectations does not happen instantaneously, which explains why we do not see an immediate drop in economic activity.

In this paper, we present an equilibrium model where crises are triggered by the emergence of new risks. Aggregate output growth is *i.i.d.* normally distributed. However, unexpectedly, the economy enters a potential recession when a new source of risk arises, leading to an anticipated temporary drop in output. The expected trajectory of output growth is U-shaped: it starts with a significant decline, followed by accelerated growth that brings output back to its pre-crisis level. Once recovery is complete, the new risk dissipates, highlighting its temporary impact on the economy. We integrate this output dynamic with a representative agent model that incorporates external habit preferences, following the approach of Menzly, Santos, and Veronesi (2004). This framework offers tractable closed-form solutions for asset prices while delivering a high equity premium and realistic return volatility.

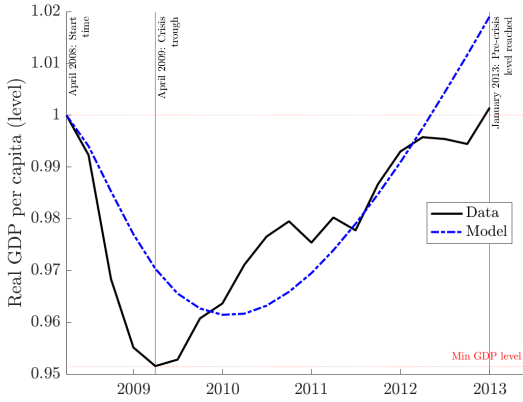
We show that in our framework, asset prices exhibit a U-shaped response to the emergence of new risks and the anticipated slowdown in economic growth. Instead of reacting immediately, expected returns display a hump-shaped pattern: risk premia temporarily rise as the crisis unfolds while current risk premia remain low. Our model captures this lagged response, consistent with empirical observations, challenging non-expected utility asset-pricing models that predict immediate market reactions (Ai and Bansal (2018)). Specifically, a model with Epstein-Zin-Weil preferences and early resolution of uncertainty, or one based on ambiguity aversion, would require an ex-ante premium for these new risks—either as compensation for not immediately knowing whether the new risk leads to a prolonged economic downturn (Ai and Bansal (2018) and Ai (2010)), or for the ambiguity arising from not knowing the precise link between news and fundamentals (Illeditsch (2011) and Illeditsch (2021)). In both cases, the unconditional premium would be too high (and increasing in the new risk sources) and

asset prices would react earlier than what is observed in the data.

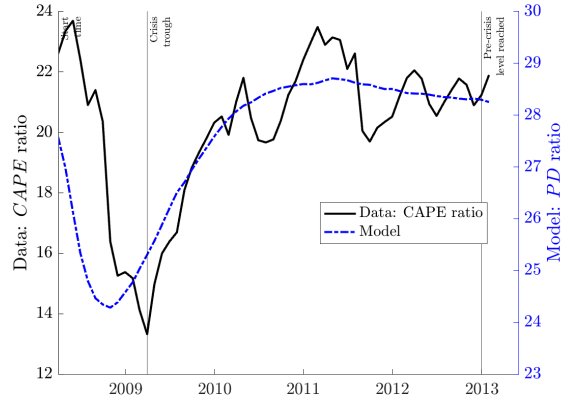
Our model rationalizes the stronger link between fundamentals and asset prices observed during crises, reflecting the increased sensitivity of financial markets to economic downturns. We demonstrate the robustness of our model by applying it to various historical periods characterized by economic downturns, showcasing its consistent ability to capture asset price dynamics during crises. We focus our analysis on the Global Financial Crisis (GFC) due to its significant global impact and data availability. We calibrate our model to match the trajectory of quarterly output level during the GFC period and the increase in output volatility observed during crises to ensure that our model produces realistic first and second moments of the simulated output, presented in Panel a) of Figure 2). We use only output data for estimation, excluding asset-pricing moments, thereby testing the model’s ability to replicate asset price dynamics. Panels b) through d) compare our model predictions for the price-dividend ratio, risk premia, and return volatility with actual data.

The predictions of our model are closely aligned with empirical evidence, accurately capturing the size, shape, and timing of key asset-pricing dynamics during crises. Specifically, the model forecasts a significant and prolonged, but not immediate, decline in the price-dividend ratio, consistent with observed data (see Panel b) of Figure 2). It also predicts a hump-shaped increase in risk premia and return volatility. This pattern mirrors the pronounced hump-shaped trajectories observed in the implied risk premium of Marfè and Pénasse (2024) and the lower bound on the equity premium of Martin (2017). Similarly, the observed return volatility exhibits a distinct hump during the GFC, further validating our model’s ability to capture these asset-pricing movements. The successful application of our model to the GFC (and other NBER-crisis periods) highlights its general applicability and effectiveness in explaining how the awareness of new priced risks affects asset prices.

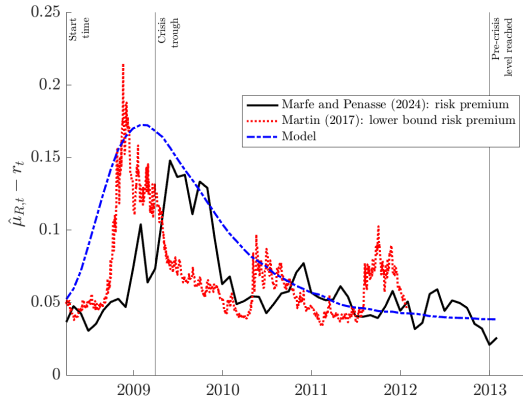
A distinguishing feature of our model is the predictable hump-shaped (or dip-shaped) patterns in asset-pricing dynamics during crises. Although there is extensive economic literature analyzing the business cycle and the shapes of output fluctuations during crises, little



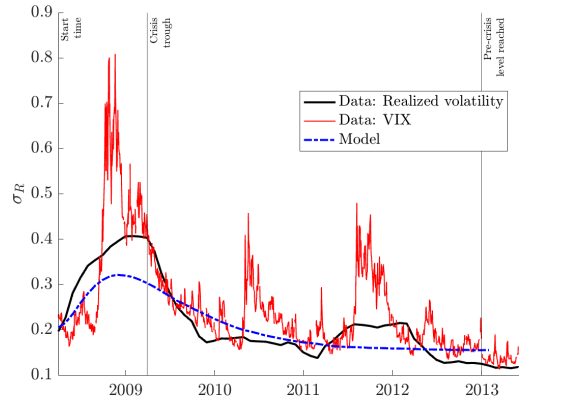
(a) Matching GDP dynamics



(b) Price-dividend ratio



(c) Risk Premium



(d) Return volatility

Figure 2. Global Financial Crisis period – Data versus Model Predictions. This figure compares model predictions (depicted by blue dashed-dotted lines) with empirical observations (shown as black and red solid lines). We compare the level of real GDP per capita in (a), the price-dividend ratio in (b), measured using the CAPE ratio, equity risk premia in (c), measured using the Marfè and Pénasse (2024) index derived from stochastic volatility and Martin (2017)’s lower bound on risk premium, and monthly realized volatility and VIX in (d), measured using the sum of daily squared returns. Section V describes how we estimate model parameters to match output data observed during the GFC period.

attention has been paid to the resulting patterns in asset prices. In the tradition of Lucas (1978), we model output dynamics to derive asset-pricing implications that directly link the behavior of asset prices to output dynamics during crises. The asset-pricing patterns during crises are driven by the time-series behavior of both the expected growth and volatility of output. As new risks arise, both the market price of risk and assets’ exposure to it increase, peaking before decreasing, which results in hump-shaped risk premia. Additionally, the

highest expected returns align with peaks in expected output volatility. Thus, our model provides a rational explanation for the delayed reaction of asset prices to recessions and their hump-shaped pattern, filling a gap in the literature by highlighting how awareness of new risks affects asset prices over time.

Our novel approach to modeling crises is motivated by two key empirical observations.¹ First, when a new risk emerges, output does not drop immediately; instead, there is a delayed decline as economic conditions gradually deteriorate over time. Second, after reaching a trough, the economy experiences a recovery phase characterized by abnormally high positive growth, with output growing faster than its long-term average. To capture both of these phenomena, we introduce a new stochastic process η , which models the gradual decline in output leading up to the crisis, as well as the accelerated growth during the recovery period. In our model, once a crisis event is triggered, output takes time to reach its minimum, reflecting the real-world lag between the emergence of new risks and their full impact on the economy. Similarly, η captures the post-crisis abnormal growth, aligning our model with empirical evidence of faster-than-average output growth during recoveries. This approach allows us to model realistic output dynamics around crises, including both the delayed drop and the subsequent rebound. In Section II, we discuss in detail the output and asset-pricing dynamics around crises observed in the data.

This paper is structured as follows. Section I discusses the related literature. In Section II, we document a number of empirical facts about the macroeconomy and asset prices around crises. Section III presents the model and Section IV the data used. We estimate the model parameters in Section V and conclude in Section VI.

¹Morley and Piger (2012) show that recessions cause large, negative, but transitory fluctuations in output. Using Hamilton (1989) model, Kim, Morley, and Piger (2005) estimate U.S. business cycle dynamics and identify a significant post-recession “bounce back” in aggregate output levels and minimal permanent effects of recessions on the U.S. economy.

I. Review of literature

Empirical facts. Recessions lead to gradual and prolonged declines in consumption (Barro and Ursúa, 2008). This trend also applies to asset prices. As noted by Muir (2017), asset prices during crises often follow a U-shaped trajectory, with cumulative returns declining by approximately 40%. However, about half of this loss is typically recovered within a few years. An analysis of 42 recessions in 14 countries since 1951 shows that both prices and dividends generally begin to decline at the start of a recession and remain significantly low even a dozen quarters after the recession ends (Kroencke, 2022).

The gradual, U-shaped response of output and other macroeconomic variables to recessions—rather than an immediate reaction—has been widely documented. Basu, Candian, Chahrour, and Valchev (2021) identify shocks to equity risk premia and show that output responds to these shocks in a similarly U-shaped pattern. Christiano, Eichenbaum, and Evans (2005) find that consumption and investment react in a hump-shaped manner following an expansionary monetary policy shock. In a Bayesian DSGE framework, Smets and Wouters (2007) generate hump-shaped responses of aggregate demand, driven by variable capital utilization and fixed production costs. Beaudry and Portier (2006) show that both consumption and stock prices respond with a pronounced hump shape to long-run TFP shocks. Finally, Brunnermeier, Palia, Sastry, and Sims (2021) estimate a structural VAR linking financial variables to economic activity and report clear hump- or dip-shaped patterns.

Our model incorporates the U-shaped pattern of output and predicts a gradual price decline, followed by a recovery period. In our model, the arrival of crises is exogenous. Supporting this, Jordà, Schularick, and Taylor (2011) find it plausible that crises emerge unpredictably. They also note considerable variations in crises regarding their effects on output and consumption, as well as their duration, features that our model effectively mirrors.

Theoretical Perspectives on Recessions and Risk Premia. Kroencke (2022) shows that innovations in expected returns are highly volatile during recessions and illustrates

that these facts are difficult to explain within standard asset pricing theories. Simulating “recessions” using frameworks like the Bansal and Yaron (2004) long-run risk model, the Campbell and Cochrane (1999) habit model, and the Wachter (2013) model of rare disasters, he observes that none of these models adequately capture the observed variances in stock prices or price changes.²

Risk premia are substantially higher in recessions than in expansions (Muir, 2017; Lustig and Verdelhan, 2012). Muir (2017) adds that risk premia spike dramatically in financial crises, defined specifically as a banking panic or banking crises, but rise only modestly in recessions or wars. Muir (2017) argues that standard consumption-based asset pricing models do not reconcile these facts because the overall drop in consumption and the increase in consumption volatility is fairly similar across financial crises and recessions and is largest during wars.³

Our model generates and matches the heightened volatility observed during recessions. Specifically, we use the observed variance ratio between crisis and non-crisis periods as a key moment to estimate the model parameters driving each crisis in our sample. The model implies not only significant increases in risk premia but also elevated return volatility, aligning closely with empirical evidence.

Nakamura, Steinsson, Barro, and Ursúa (2013) estimate an empirical model of consumption disasters, which generates an equity premium from disaster risk that is substantially smaller than in disaster models. They conclude that an unrealistically large value of the inter-temporal elasticity of substitution is necessary to explain stock-market crashes at the onset of disasters. Gourio (2012) introduces time-varying disaster risk into a standard real business cycle model, which is also capable of generating a U-shaped reaction of macroeconomic variables and asset prices. His approach, however, relies on leverage to generate

²For a detailed review of the implications of disaster risk for asset pricing, see Tsai and Wachter (2015).

³More recent literature offers clues on the potential mechanism driving the higher expected returns observed during recessions. Ai and Bhandari (2021) show that when idiosyncratic risk to human capital is not fully insurable, the anticipation of lack of risk sharing in the future can raise workers’ current marginal utilities during recessions.

volatility of cash flows and returns, and it does not address the volatility of the unlevered return on capital.

Ghaderi, Kilic, and Seo (2022)'s model of slowly unfolding disasters explains the gradual response of asset prices to economic shocks through information processing. In this framework, agents learn about the time-varying intensity of consumption jumps, which increases during disasters. The process of recognizing a sustained transition to a recessionary state contributes to the prolonged effects associated with disasters. In contrast to our model, Ghaderi, Kilic, and Seo (2022)'s gradual response of asset prices is not driven by the output dynamics observed during crises, but is instead the result of agent learning about consumption jumps.

The post-crisis period is associated with abnormally high economic growth, also known as the bounce-back effect in level (Nakamura, Steinsson, Barro, and Ursúa, 2013; Kim, Morley, and Piger, 2005). Classical asset-pricing models, including the Ghaderi, Kilic, and Seo (2022)'s slowly unfolding disasters model, do not generate this recovery period. Beeler and Campbell (2012) show the long-run risk model produces persistence but not mean reversion in the level of consumption. Hasler and Marfè (2016) highlight the importance of recoveries that follow disaster events in explaining the observed shape of the term structures of equity return.

Our model contributes to the existing body of literature studying the relationship between crises and their ensuing impacts on asset prices and economic activity. We show that during economic recessions, the connection between asset prices and fundamentals becomes significantly stronger. Using a novel general equilibrium model, we explain why asset prices do not respond immediately to the introduction of new risks, even in the face of an anticipated economic slowdown. Our model predictions can quantitatively match the asset price reactions, which manifest in a hump-shaped pattern of expected returns and return volatility. The paper sets itself apart from other existing theories by demonstrating that the model can mirror actual recession dynamics, both in terms of changes in observed levels of output

and risk premia.

II. Empirical facts

In this section, we discuss empirical stylized facts of output, crisis heterogeneity, and asset prices during different phases of the business cycle.

A. The U-shaped output during crises

Figure 3 shows the evolution of US production over the past 70 years, highlighting that recessions have consistently created significant economic disruptions. These periods generate large output gaps due to substantial drops in total output, while there are no similar positive shocks. This asymmetric feature, first documented by Neftci (1984), is a reason why the National Bureau of Economic Research (NBER) focuses on identifying and studying recessions. While this asymmetry is well-documented in the data, our model in Section III explicitly incorporates it as a novel feature.

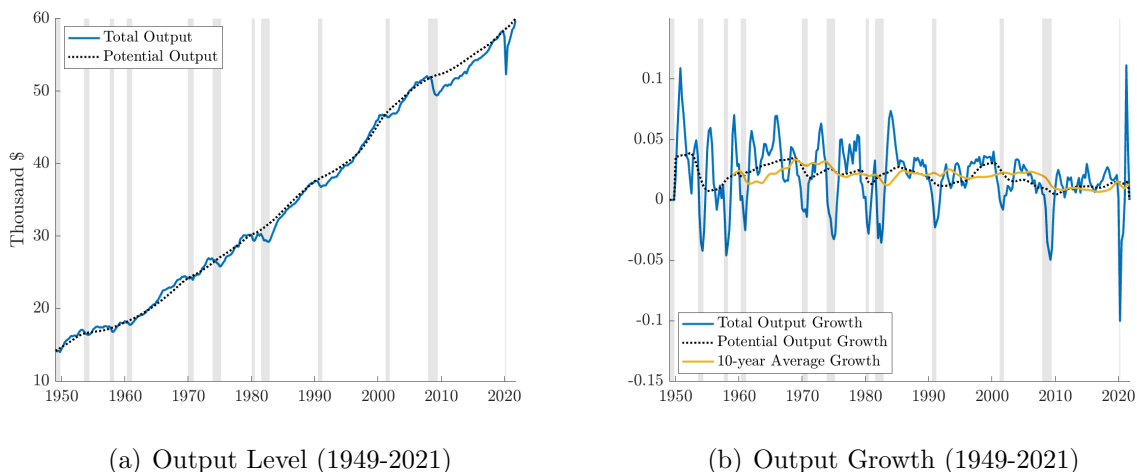


Figure 3. Real GDP per capita (1949-2021) Panel (a) displays the evolution of the quarterly real and potential output in the United States (per capita) between 1949 to 2021. In panel (b), the figure shows the year-on-year change in the quarterly GDP and potential output (the blue and dashed black line, respectively) as well as the 10-year average total GDP growth rate (yellow line). Shaded areas represent NBER recessions.

Since the 1990s, growth has been more moderate compared to previous decades, a trend attributed by Fernald (2015) to a mid-2000s slowdown in labor productivity. Despite this moderation, negative shocks during NBER recession periods continue to have a substantial impact on output dynamics. To account for these varying growth trends, we measure abnormal growth as the deviation of actual growth in a given quarter from the historical 10-year average. This measure provides a clearer picture of the deviations around crises. The left plot of Figure 4 shows abnormal growth for U.S. output from 1950 to 2021. Abnormal growth is typically negative leading to crises (as highlighted by the red arrows) and becomes positive during recoveries (as highlighted by the green arrows), reinforcing the asymmetry observed in business cycles.

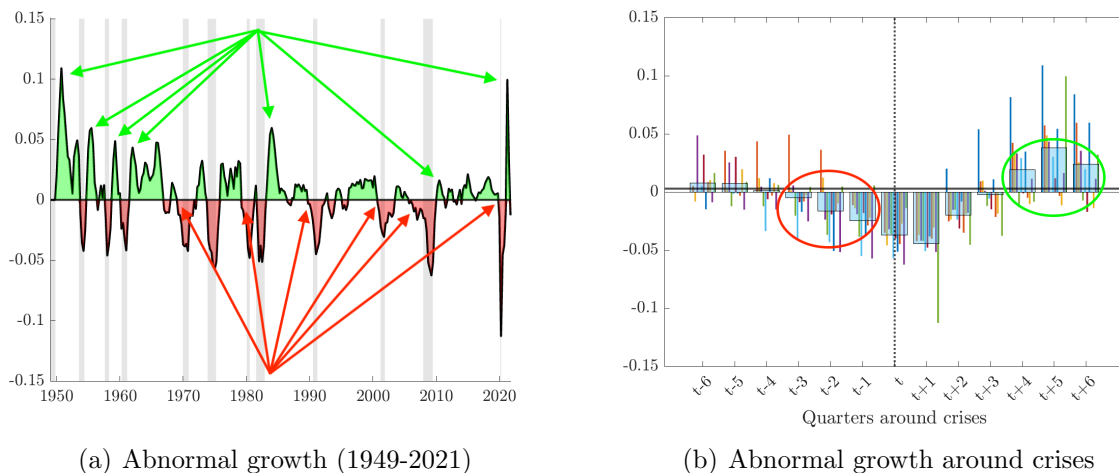


Figure 4. Abnormal output growth (1949-2021). The figure displays the level of abnormal growth measured as the difference between the realized annual growth rate of the real GDP per capita and the 10-year historical average output growth. Panel (a) describes the time series evolution of abnormal growth from 1949 until 2021. Shaded areas reflect NBER recessions. Panel (b) shows the average evolution of abnormal growth around crisis driver dates, i.e., it displays the aggregated average abnormal growth levels up to six quarters before and after the beginning of each NBER recession. The wide transparent blue bars represent the aggregate average dynamics. The narrow bars in color describe the individual NBER crisis observations covered in our sample.

We aggregate pre- and post-crisis periods to compute the average abnormal growth rate for up to six quarters before and after a crisis. The right plot of Figure 4 shows this trend, with the red circle highlighting the gradual decline in abnormal growth preceding the official

start of NBER recessions and the green circle marking the positive abnormal growth observed after the crisis. On average, after a year, the economy enters a recovery phase where realized output eventually catches up to potential output. This catch-up occurs within a few years and post-crisis growth often exceeds normal levels compared to the historical 10-year average growth rate, highlighted by the green circle on the right graph of Figure 4. Consistent with these observations, Bordo and Haubrich (2017) confirm that U.S. recessions are typically followed by rapid recoveries, except in three cases: the Great Contraction in the 1930s, the early 1990s recession and the Global Financial Crisis.

B. Heterogeneity across economic crises

Historical evidence highlights that crises differ significantly in their characteristics, including duration, severity, and post-crisis recovery dynamics. Figure 5 documents the duration (in years) and severity (measured as a drop in output at the crisis trough) of all NBER-designated recessions from 1947 until 2024. Using the NBER method, we identify and date 12 recognized crises from 1947 to 2024. Unlike the NBER, a crisis ends for us when real quarterly output returns to pre-crisis levels, covering 30.97% of quarters as crisis periods. On average, it takes about a year to reach a crisis trough and two years to fully bounce back to pre-crisis output levels.

Figure 5 compares the severity and duration of the 12 recessions included in our sample. Crisis severity is defined as the percentage decline in output at the trough (lowest point) relative to the recession’s start date. Panel (a) shows that the most severe recession is the COVID-19 recession, followed by the Great Recession. Panel (b) illustrates the output dynamics of each recession, measuring the duration from the start to the trough and from the trough to recovery back to pre-crisis levels. The light gray bars represent the “start to trough” period, while the darker bars indicate the “trough to recovery” period.

While the COVID-19 recession in 2020 was one of the shortest recessions on record, it caused an unprecedented GDP contraction of almost 10%, highlighting that short crises can

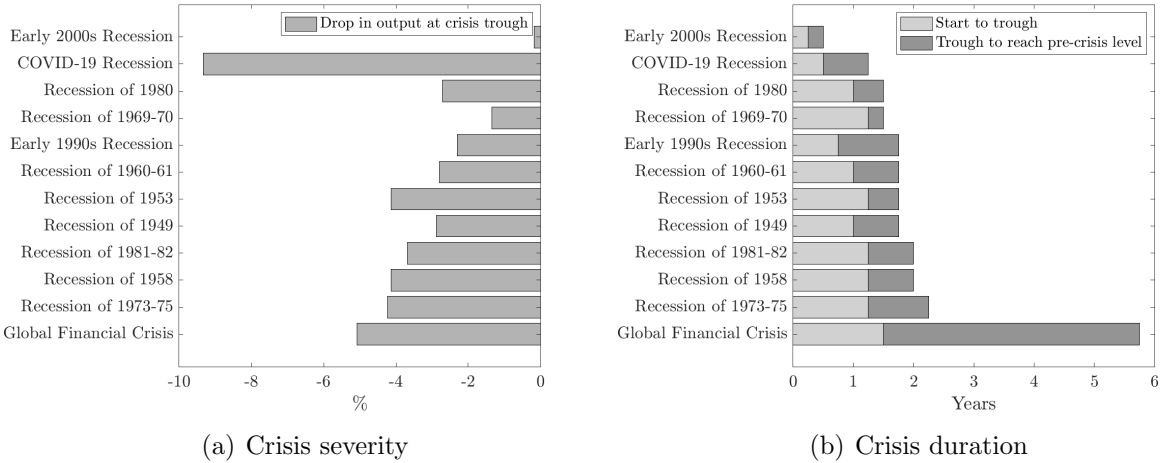


Figure 5. Crisis characteristics. The figure highlights the differences in both the depth of the economic downturns and the length of the recovery periods across various recessions. Panel (a) shows the severity of economic recessions, represented by the percentage drop in output at the lowest point of each crisis. Panel (b) illustrates the duration of these recessions, with light gray bars representing the period from the start to the trough, and dark gray bars representing the period from the trough to recovery.

also cause substantial economic damage. In contrast, the Global Financial Crisis lasted more than five years, with cumulative losses far exceeding most downturn periods.

Understanding this heterogeneity is critical for modeling the impact of crises on asset prices. More severe crises, with larger GDP declines and slower recoveries, are likely to impose greater downward pressure on asset valuations. Furthermore, the speed of mean reversion in output after a crisis varies across episodes, with some crises exhibiting rapid recoveries, while others (e.g., the Global Financial Crisis) are marked by prolonged stagnation or sluggish rebounds.

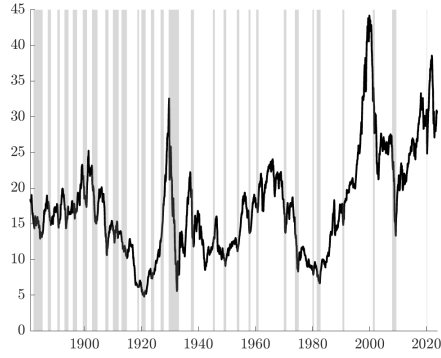
Our asset-pricing model in Section III accounts for this crisis-specific variation by incorporating heterogeneous output dynamics following economic shocks. Specifically, differences in recovery speeds and the magnitude of economic disruptions directly influence the evolution of key risk factors that determine asset prices.

C. Asset prices around crises

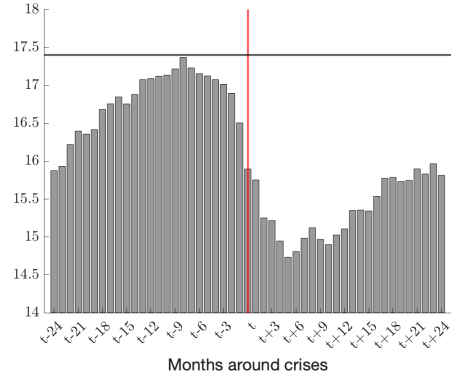
How do asset prices respond to recessions? Figure 6 provides a detailed view of how stock market valuations, risk premia, and return volatility evolve around crises. The top left plot shows the time series of the Shiller CAPE ratio, a measure of stock market valuations, from 1881 to 2024. It illustrates how valuations fluctuate over time, with notable drops during major economic crises. The left middle plot highlights stock market risk premia, with the red line representing the Marfè and Pénasse (2024) measure and the blue line showing the Martin (2017) implied lower bound. Finally, the plot in the bottom left shows the time series of the VIX, an indicator of market volatility, from 1990 to 2021.

The right-hand plots examine the behavior of these variables around crises, aggregating data from 24 months before to 24 months after the start of each NBER-designated recession. The top right graph illustrates the U-shaped pattern of the CAPE ratio, showing an initial decline during crises followed by a gradual recovery as markets stabilize and valuations rebound. The middle right plot focuses on the Marfè and Pénasse (2024) measure of risk premia, which exhibits a hump-shaped pattern. Risk premia rise gradually at the onset of a recession, peaking shortly after the crisis begins, before slowly reverting toward steady-state levels during the recovery phase. This behavior contrasts with regime-switching models, where risk premia adjust instantaneously. The bottom right plot highlights the VIX dynamics, which tend to peak just before or around the official start of recessions and remain elevated for an extended period, often lasting up to two years. However, the VIX patterns are noisier and less consistent than the other variables, as this measure aggregates data from only four NBER recessions.

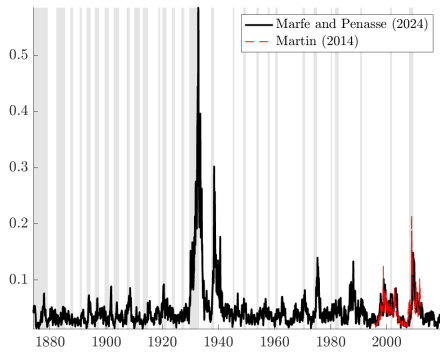
These patterns reveal key stylized facts about asset prices during crises. For instance, while the Dot-com bubble saw minimal changes in risk premia, the Great Recession triggered a much larger and more prolonged increase. Similarly, the VIX response varies by crisis, with particularly high and prolonged spikes during the Global Financial crisis and the COVID-19 pandemic. The U-shaped behavior of the CAPE ratio and the hump-shaped dynamics



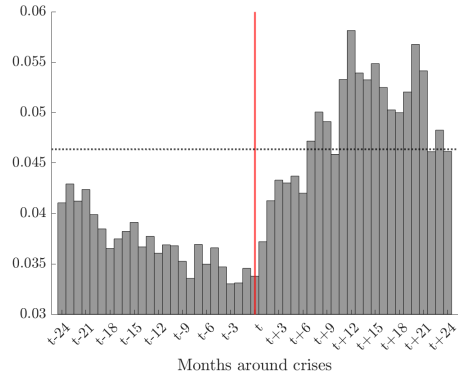
(a) CAPE (1881-2024)



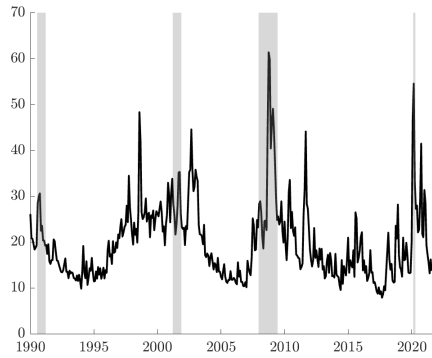
(b) CAPE around crises



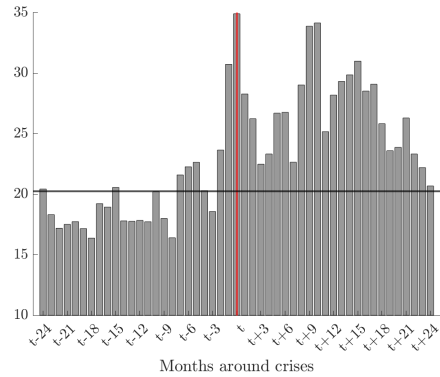
(c) Risk premia (1874-2017)



(d) Risk premia (Marfè and Pénasse, 2024) around crises



(e) VIX (1990-2021)



(f) VIX around crises

Figure 6. Asset prices around crises. The figure displays the CAPE ratio, risk premia, and return volatility, measured using the VIX index. We plot the development of the monthly levels of the CAPE ratio (Figure (a)), risk premia (Figure (c)), and VIX (Figure (e)) over time, as well as their conditional levels observed in months before and after NBER crises (in Figures (b), (d), and (f), respectively).

of risk premia and volatility highlight the need to account for crisis-specific dynamics in asset-pricing models, a challenge we address in the next section.

III. The Model

In this section, we derive equilibrium asset prices in an exchange economy that captures business-cycle dynamics through realistic output fluctuations observed during crises. We introduce a time variation in risk aversion by endowing the representative investor with external habit-forming preferences to better match unconditional moments of asset prices.

A. Output

Our model’s main innovation is incorporating output patterns during crises into the output process via two interconnected processes: η_t , defined below in Equation (3) and referred to as the crisis impact, and x_t , defined below in Equation (4) and referred to as the crisis driver. The crisis driver (x_t) captures the expected trajectory of the economic disruption due to the new source of risk,⁴ while the impact of the crisis (η_t) reflects the immediate and dynamic response of output to this disruption. Specifically, we decompose the output as follows.

$$Y_t = \hat{Y}_t \eta_t, \tag{1}$$

where \hat{Y}_t represents output under normal economic conditions (e.g., \hat{Y}_t can be viewed as potential output when firms operate at full capacity). The process \hat{Y}_t follows a geometric Brownian motion

$$d\hat{Y}_t = \mu_{\hat{Y}} \hat{Y}_t dt + \sigma_{\hat{Y}} \hat{Y}_t dZ_{\hat{Y},t}, \tag{2}$$

where $\mu_{\hat{Y}}$ and $\sigma_{\hat{Y}}$ are constants and $Z_{\hat{Y},t}$ is a Brownian shock.

The crisis impact, η_t , is a strictly positive stochastic process that depends on a two-state

⁴We use the term ‘new risks’ to refer to crisis-specific shocks that alter the path of output and risk premia. These are modeled via crisis-specific calibrations to capture observed heterogeneity across recessions.

continuous-time Markov process $\omega_t \in \{H, L\}$. In normal economic times, $\omega_t = H$, $\eta_t = 1$, and thus output growth is i.i.d. normally distributed. When a crisis occurs at random time s , $\omega_t = L$, η_t becomes stochastic and typically falls below one, reflecting the negative impact on output Y_t .

Transitions from the normal state H to the crisis state L occur at a random arrival time s that is exponentially distributed with intensity parameter ν . Once a crisis begins at time s , the crisis impact, η_t , evolves for all $t \geq s$ according to:

$$d\eta_t = \kappa_\eta (x_t - \eta_t) dt + \sigma_\eta \eta_t (\lambda - \eta_t) dZ_{\eta,t}, \quad (3)$$

where $\kappa_\eta > 0$, $\sigma_\eta > 0$, $\lambda > 1$, and $Z_{\eta,t}$ is a Brownian shock. The instantaneous volatility term, $\sigma_\eta \eta_t (\lambda - \eta_t)$, ensures that η_t remains within the interval $(0, \lambda)$, given that $\lambda > 1$. The initial and terminal conditions for the crisis-impact process are $\eta_s = \eta_\tau = 1$, where τ denotes the end of the crisis defined in Equation (5).

The crisis impact, η_t , is reverting towards the crisis driver, x_t , where x_t is given by

$$x_t = 1 - \left(e^{-\kappa_1(t-s)} - e^{-\kappa_2(t-s)} \right) \varepsilon, \quad \forall s \leq t \leq \tau \quad (4)$$

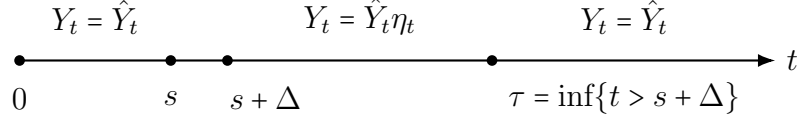
where $0 < \kappa_1 < \kappa_2$ and $\varepsilon > 0$. The crisis driver x_t follows a U-shaped pattern: it starts at one, decreases to a minimum, and then reverts back towards one, as shown in Figure 7. This reflects temporary output destruction during crises, followed by above-average growth during recovery.⁵

The crisis ends at the stopping time τ , defined as:

$$\tau = \inf \{ t > s + \Delta, \quad \text{s.t.} \quad \eta_t = 1 \}, \quad (5)$$

⁵Gârleanu and Panageas (2015) use a similar approach with the sum of two negative exponential functions to model the hump-shaped pattern of earnings, while Blanchard (1985) applies the same functional form to capture complex household income paths in Footnote 8.

where the strictly positive parameter Δ ensures that η_t does not immediately return to 1 at time s , preventing the emergence of a crisis. Intuitively, Δ captures the time it takes for the crisis to fully impact the economy and for agents to adjust their expectations. The timeline below describes the evolution of output during a crisis starting at time s .



There are several important aspects of the crisis impact process in Equation (3): (i) when the economy enters the crisis state L , a new Brownian motion, $Z_{\eta,t}$, emerges, affecting output and becoming priced; (ii) both the mean and volatility of output growth become stochastic; (iii) output volatility jumps at time s since $\lambda > 1$, even though the output level does not; and (iv) setting $\lambda > 1$ ensures the economy exits the crisis state in finite time τ .

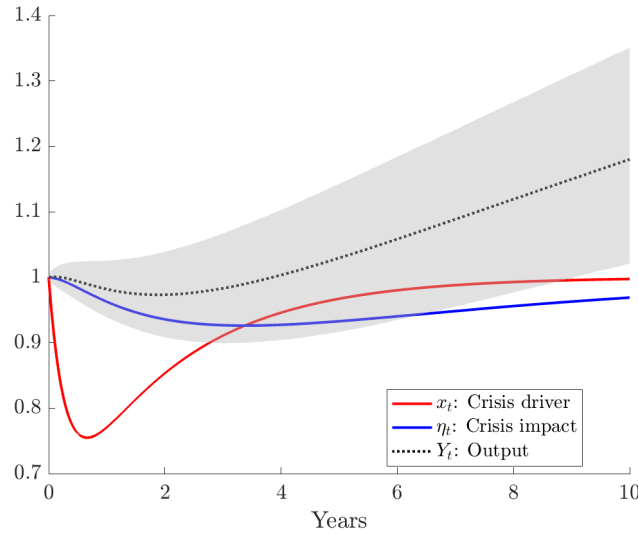


Figure 7. Crisis-driver (x_t) and crisis-impact (η_t) variables. The red line shows the crisis-driver variable x_t that responds to an initial shock $\varepsilon = 0.4$. The blue line describes the output reaction to the crisis, represented by η_t . The shaded area represents the 5-95% confidence bands for the simulated Y_t paths. The parameters are set to $\mu_{\hat{Y}} = 0.0197$, $\sigma_{\hat{Y}} = 0.0254$, $\kappa_{\eta} = 0.2$, $\lambda = 1.01$, $\sigma_{\eta} = 0.3$, $\kappa_1 = 0.5$ and $\kappa_2 = 3.4$.

Figure 7 shows the crisis driver, x_t (red line), the average path of the crisis impact, η_t (blue line), and output, Y_t (black dotted line with shaded 5-95% confidence bands). The U-shaped pattern of x_t , along with η_t catching up to it, suggests that both η_t and aggregate output

follow similar dynamics. These U-shaped output patterns during recessions and recoveries may result from gradual adjustments in capital and labor inputs, as well as inter-temporal smoothing by households with borrowing constraints.

This delayed reaction of output is chosen on purpose to fit the dynamics of output around crises. In data, we observe that the drop in realized output is not instantaneous. In fact, in Figure 4 we show that abnormal growth, which measures the difference between the realized GDP growth and a 10-year historical average GDP growth, drops in a gradual manner. This gradual drop in output growth is followed by the ‘bounce-back’ effect, where the abnormal growth becomes positive. Both features of the aggregate output data are consistent with our model.

The left plot of Figure 8 shows the crisis driver x_t (red line), while the right plot shows the average path of the crisis impact, η_t , (blue line with shaded 5-95% confidence bands) for different initial shocks $\varepsilon \in \{0.05, 0.2, 0.4\}$. Larger initial shocks lead to more severe and prolonged recessions. The response of x_t to the initial shock is sharper than that of η_t , which is expected since η_t adjusts to x_t over time, depending on κ_η .

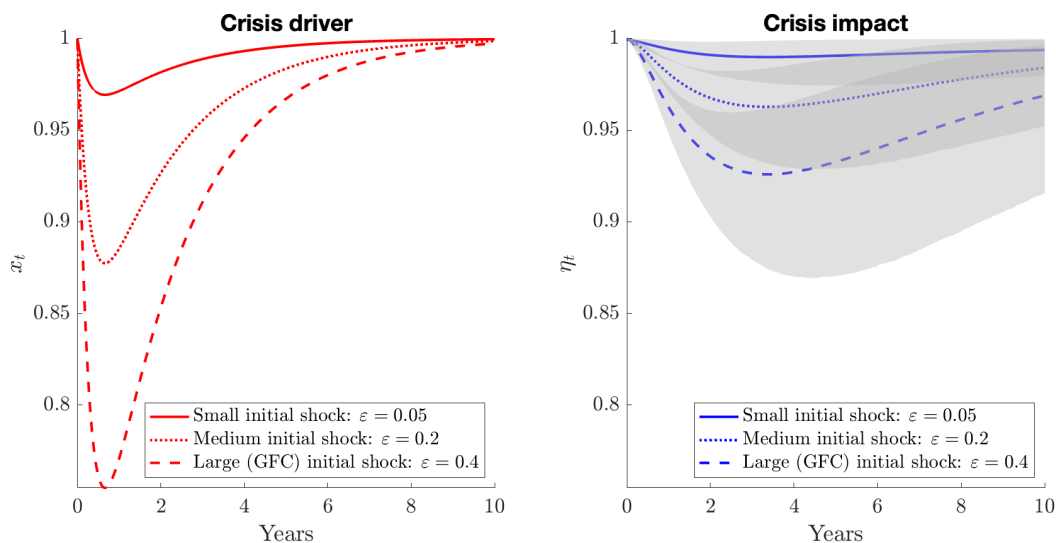


Figure 8. Crisis driver and crisis impact for different initial crisis shocks. The red line shows x_t and the blue line depicts η_t for different levels of the shock ε , that is, 0.05, 0.2, and 0.4, with shaded areas around η_t representing 5-95% confidence bands. The parameters are set to $\kappa_\eta = 0.2$, $\lambda_\eta = 1.01$, $\sigma_\eta = 0.3$.

Figure 9 illustrates how the parameter κ_η (in panel (a)) influences the behavior of the crisis impact η_t . The red line shows the crisis driver x_t , the blue solid line shows the average path of the crisis impact, η_t , when $\kappa_\eta = 0.5$ (with shaded 5-95% confidence bands), and the blue dashed line shows the average path of the crisis impact, η_t , (with shaded 5-95% confidence bands) when $\kappa_\eta = 3$, $\kappa_1 = 0.5$ and $\kappa_2 = 3.4$. When κ_η is higher, η_t tracks the path of the crisis driver x_t more closely, leading to faster recoveries and shorter recessions. In contrast, lower values of κ_η result in slower adjustments of η_t to x_t , prolonging the recession and delaying recovery.

Increasing the levels of κ_1 , κ_2 , and their ratio (κ_2/κ_1) also impacts the severity and duration of crises, similarly to an increase in κ_η , as shown in panel (b) of Figure 9. This indicates that all three κ parameters are important determinants of crisis characteristics, which can differ significantly across recessions.

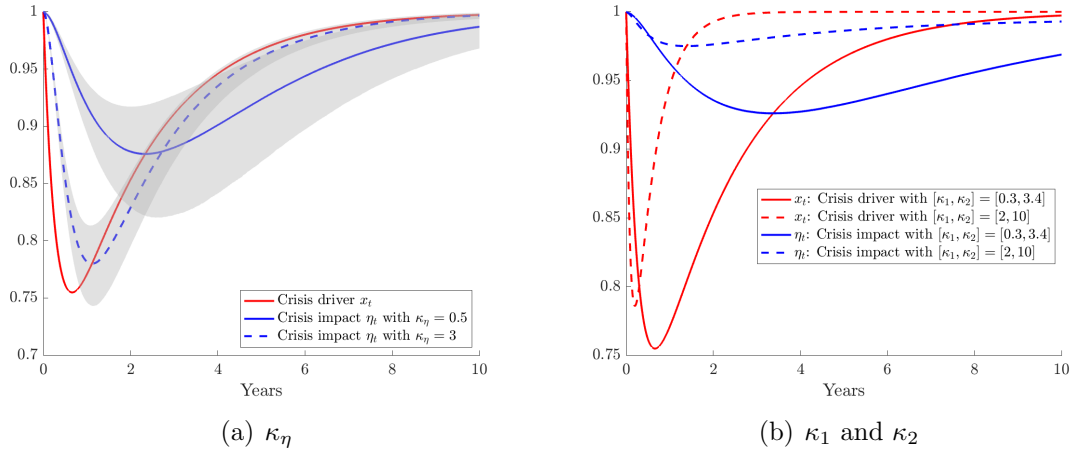


Figure 9. Crisis driver and crisis impact for different κ_i parameters. Panel (a) displays x_t and η_t for different levels of κ_η , that is, 0.5 and 3, with shaded areas around η_t representing 5-95% confidence bands, with $\kappa_1 = 0.5$ and $\kappa_2 = 3.4$. Panel (b) shows x_t and η_t for different levels of $[\kappa_1, \kappa_2]$, that is, $[0.3, 3.4]$ and $[2, 10]$, with $\kappa_\eta = 0.2$. The remaining parameters are set to $\varepsilon = 0.4$, $\lambda = 1.01$, $\sigma_\eta = 0.3$, in both panels.

Deeper and more persistent crises, which cause long-lasting damage, can be generated in this model by a combination of a large initial shock ε and low κ parameters. This aligns with empirical evidence that severe crises often take longer to resolve. By incorporating these dynamics, the model allows us to distinguish between different types of recession events. For

example, financial crises often exhibit greater severity and persistence compared to non-financial crises, and these distinctions are reflected in their varying impacts on asset prices (Reinhart and Rogoff, 2009).

B. Asset pricing

In this section, we determine the price, expected return, and volatility of the market portfolio, along with the risk-free rate, and analyze their behavior during crises. In our framework, the asset-pricing patterns emerge directly from the U-shaped dynamics in expected output growth and volatility. This transmission mechanism offers a clean mapping from macro dynamics to asset returns. Initially, we use a stochastic discount factor (SDF) as in Menzly, Santos, and Veronesi (2004), which results in hump-shaped stock market risk premia and volatilities, while the price-dividend ratio remains relatively flat. Therefore, in Section III.C, we explore a model with amplified risk aversion, where during a crisis, risk aversion is influenced by both normal and emerging output shocks, and its long-run mean is more closely tied to output dynamics. All proofs are provided in Appendix A.

B.a. Preferences

We consider a representative agent (RA) who maximizes

$$\mathbb{E}_0 \left[\int_0^\infty u(C_t, H_t, t) dt \right] = \mathbb{E}_0 \left[\int_0^\infty e^{-\rho t} \log(C_t - H_t) dt \right], \quad (6)$$

where C_t is consumption, ρ is the time discount rate, and $H_t = C_t(1 - 1/\mathcal{R}_t)$ is an external habit. We refer to \mathcal{R}_t as (conditional) risk aversion, since the local coefficient of relative risk aversion is

$$\mathcal{R}_t \equiv -\frac{u_{CC}(C_t, H_t, t)C_t}{u_C(C_t, H_t, t)} = \frac{C_t}{C_t - H_t}. \quad (7)$$

Rather than modeling the dynamics of the inverse surplus consumption ratio (\mathcal{R}_t) as in Campbell and Cochrane (1999), we follow Menzly, Santos, and Veronesi (2004) and let risk

aversion \mathcal{R}_t evolve as a mean-reverting process that is perfectly (locally) negatively correlated with consumption growth. Specifically,

$$d\mathcal{R}_t = \kappa_{\mathcal{R}} (\bar{\mathcal{R}} - \mathcal{R}_t) dt - \alpha (\mathcal{R}_t - \lambda_{\mathcal{R}}) \left(\frac{dC_t}{C_t} - \mathbb{E}_t \left(\frac{dC_t}{C_t} \right) \right), \quad (8)$$

where $\bar{\mathcal{R}} > \lambda_{\mathcal{R}} > 0$ ensures that \mathcal{R}_t is bounded below by the parameter $\lambda_{\mathcal{R}} > 0$. The parameter $\kappa_{\mathcal{R}} > 0$ is the speed of mean reversion in \mathcal{R}_t ; a lower $\kappa_{\mathcal{R}}$ implies that consumption shocks have a more persistent impact on risk aversion because \mathcal{R}_t takes longer to revert to its long-run mean. The strictly positive parameter α governs how negative consumption shocks raise risk aversion \mathcal{R}_t ; a larger α implies a higher volatility of risk aversion \mathcal{R}_t .

Finally, the conditional expectation of future risk aversion is

$$\mathbb{E}_t [\mathcal{R}_u] = \bar{\mathcal{R}} + (\mathcal{R}_t - \bar{\mathcal{R}}) e^{-\kappa_{\mathcal{R}}(u-t)}, \quad \forall u > t. \quad (9)$$

Over any sufficiently long horizon, the economy may switch multiple times between normal and crisis regimes. Consequently, \mathcal{R}_t is exposed to distinct Brownian shocks— $Z_{\hat{Y},t}$ in normal times and $Z_{\eta,t}$ in crises. Nonetheless, the conditional expectation $\mathbb{E}_t[\mathcal{R}_u]$ does not depend on how often these transitions occur. As long as the current level \mathcal{R}_t is known, the process ultimately reverts toward the same constant long-run mean $\bar{\mathcal{R}}$, as in Menzly, Santos, and Veronesi (2004).⁶ Hence, even though \mathcal{R}_t path-wise reflects the sequence of shocks in normal and crisis states, its conditional expectation depends solely on the current value of \mathcal{R}_t .

We relax this assumption in Section III.C, allowing \mathcal{R}_t to revert toward a time-varying mean, $\bar{\mathcal{R}}_t$, which depends on the crisis driver x_t . This additional feedback further raises risk aversion during crises, and thus aligns more closely with the notion of habit intensifying in distressed periods.

⁶ $\bar{\mathcal{R}}$ is the unconditional long-run mean of \mathcal{R}_t because if we let time t in Equation (9) start in the infinite past we have that

$$\lim_{t \rightarrow -\infty} \mathbb{E}_t[\mathcal{R}_u] = \bar{\mathcal{R}}.$$

B.b. The stochastic discount factor

Upon imposing market clearing ($C_t = Y_t$) and using the marginal utility of the RA as the pricing kernel M_t , the stochastic discount factor (SDF) is

$$M_t = e^{-\rho t} \frac{1}{Y_t - H_t} = e^{-\rho t} \frac{\mathcal{R}_t}{Y_t}. \quad (10)$$

The term $e^{-\rho t}/C_t$ corresponds to the classical log-utility SDF, where $e^{-\rho t}$ captures time discounting, and marginal utility is higher in states with lower aggregate consumption C_t . The term \mathcal{R}_t (the inverse surplus consumption ratio) amplifies the marginal utility when C_t is close to the habit level H_t . In such states, $(C_t - H_t)/C_t$ (the surplus consumption ratio) is small, implying a higher \mathcal{R}_t and thus further discounting.

Importantly, because C_t does not jump when the economy transitions into or out of a crisis, the random times s and τ are not priced with log-utility.⁷ Therefore, applying Itô's lemma to M_t given in Equation (10) leads to the risk-free rate and the market prices of risk presented in the next proposition.

Proposition 1: *The dynamics of the equilibrium stochastic discount factor, M_t , are*

$$\frac{dM_t}{M_t} = -r_t dt - \theta_{\hat{Y},t} dZ_{\hat{Y},t} - \theta_{\eta,t} dZ_{\eta,t}. \quad (11)$$

In equilibrium the risk-free rate is

$$r_t = r^{log} + r_t^{habit} + \begin{cases} r_t^{crisis} & \text{if } \omega_t = L \\ 0 & \text{if } \omega_t = H, \end{cases} \quad (12)$$

where $r^{log} = \rho + \mu_{\hat{Y}} - \sigma_{\hat{Y}}^2$ is the constant log-utility component and $r_t^{habit} = \kappa_{\mathcal{R}} \left(1 - \frac{\bar{\mathcal{R}}}{\mathcal{R}_t}\right) - \alpha \left(1 - \frac{\lambda_{\mathcal{R}}}{\mathcal{R}_t}\right) \sigma_{\hat{Y}}^2$ is the habit-driven component. The new crisis term that only appears when

⁷While the output level does not jump at these times, the conditional output distribution does change, so such events can be priced under alternative preferences (e.g., Epstein-Zin-Weil preferences).

$\omega_t = L$ is

$$r_t^{crisis} = \kappa_\eta (x_t/\eta_t - 1) - \sigma_\eta^2 (\lambda - \eta_t)^2 - \alpha \left(1 - \frac{\lambda \mathcal{R}}{\mathcal{R}_t}\right) \sigma_\eta^2 (\lambda - \eta_t)^2. \quad (13)$$

The market price of risk for the Brownian shock $Z_{\hat{Y},t}$ is

$$\theta_{\hat{Y},t} = \sigma_{\hat{Y}} \left(1 + \alpha \left(1 - \frac{\lambda \mathcal{R}}{\mathcal{R}_t}\right)\right). \quad (14)$$

The market price of risk for the Brownian shock $Z_{\eta,t}$ is

$$\theta_{\eta,t} = \begin{cases} \sigma_\eta (\lambda - \eta_t) \left(1 + \alpha \left(1 - \frac{\lambda \mathcal{R}}{\mathcal{R}_t}\right)\right) & \text{if } \omega_t = L \\ 0 & \text{if } \omega_t = H. \end{cases} \quad (15)$$

The left plot in Figure 10 shows the market prices of risk. The average $\theta_{\hat{Y},t}$, represented by the solid blue line with 5 – 95% confidence bands, remains relatively flat during the crisis, although its volatility significantly increases during the first two years of the new risk source before stabilizing. In contrast, the market price of the new risk source η_t exhibits a hump-shaped pattern, skewed to the right, with the right tail peaking almost three times the average after three years. While the average $\theta_{\hat{Y},t}$ maintains a modestly declining trend, the awareness of the new risk source significantly amplifies overall risk compensation, driving it upward in a pronounced hump-shaped trajectory. This dynamic highlights the critical role of the new risk source in reshaping risk premia during crises.

Awareness of a new source of risk also affects the risk-free rate, as illustrated in the right graph in Figure 10. The black solid line represents the constant risk-free rate that would prevail under i.i.d. consumption growth with a log-utility representative agent. The green line captures the additional habit-driven component introduced by habit-formation preferences. Once a crisis emerges, the red line shows a further decline in the risk-free rate, reflecting lower expected output growth and stronger precautionary savings. As the crisis subsides and the growth recovers, precautionary savings diminish, pushing the rate back up, thus producing a “U”-shaped pattern (blue line) for the overall risk-free rate.

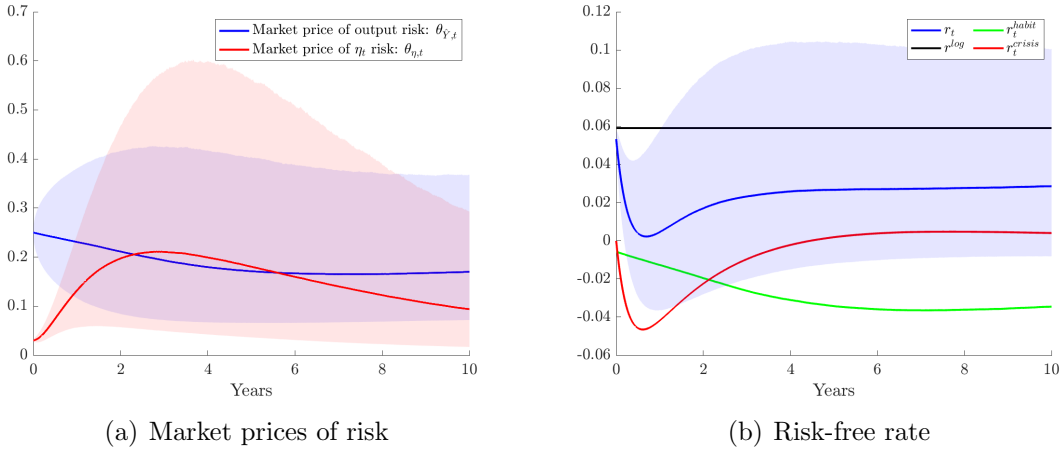


Figure 10. Market prices of risk and risk-free rate. Panel (a) shows the time-series evolution of the market prices of the ‘normal’ output risk ($\theta_{\hat{Y},t}$) in blue and η_t risk ($\theta_{\eta,t}$) in red. Panel (b) displays the time-series evolution of the equilibrium risk-free rate and its individual components in a crisis state, i.e., when $s < t + \Delta < \tau$. The total real risk-free rate, r_t , is in blue. This risk-free rate can be decomposed into three components: $r_t = r_t^{log} + r_t^{habit} + r_t^{crisis}$. Parameters used to create this figure are the following: $\mu_{\hat{Y}} = 0.0197$, $\sigma_{\hat{Y}} = 0.0254$, $\rho = 0.04$, $\kappa_{\mathcal{R}} = 0.16$, $\lambda_{\mathcal{R}} = 22$, $\bar{\mathcal{R}} = 34$, $\alpha = 25.125$, $\kappa_1 = 0.5$, $\kappa_2 = 3.4$, $\varepsilon = 0.4$, $\kappa_{\eta} = 0.2$, $\sigma_{\eta} = 0.3$ and $\lambda = 1.01$. Shaded areas represent 5-95% confidence bands.

B.c. The stock market

The market portfolio is a claim on the aggregate output stream. Consequently, its price is

$$S_t = \mathbb{E}_t \left[\int_t^{\infty} \frac{M_u}{M_t} Y_u du \right] = \phi_t Y_t, \quad (16)$$

where ϕ_t is the price-dividend ratio. Substituting the SDF from Equation (10) into Equation (16), changing the order of integration and expectation, and using Equation (9) for the conditional expectation of risk aversion leads to

$$\phi_t = \int_t^{\infty} e^{-\rho(u-t)} \mathbb{E}_t \left[\frac{\mathcal{R}_u}{\mathcal{R}_t} \right] du = \int_t^{\infty} e^{-\rho(u-t)} \left(\frac{\bar{\mathcal{R}}}{\mathcal{R}_t} + \left(1 - \frac{\bar{\mathcal{R}}}{\mathcal{R}_t} \right) e^{-\kappa_{\mathcal{R}}(u-t)} \right) du. \quad (17)$$

Equation (17) shows that the price-dividend ratio depends entirely on the time discount rate ρ and the current level of risk aversion \mathcal{R}_t with its long-run mean $\bar{\mathcal{R}}$ and speed of mean reversion $\kappa_{\mathcal{R}}$. Neither the crisis state nor the frequency of regime transitions enter explicitly. Intuitively, once \mathcal{R}_t is known, the conditional expectation of future risk aversion is pinned

down by Equation (9), so additional information about the timing of the crisis does not alter ϕ_t . Evaluating the integral in Equation (17) completes the derivation of the price dividend ratio. Then, applying Itô's lemma to $S_t = Y_t \phi_t$, provides the instantaneous expected return and volatility of the market portfolio, as summarized in the next proposition.

Proposition 2 (Market Portfolio): *In equilibrium, the price of the market portfolio is $S_t = Y_t \phi_t$. The price-dividend ratio is*

$$\phi_t = \frac{1}{\rho} \left(\frac{\bar{\mathcal{R}}}{\mathcal{R}_t} + \frac{\rho}{\rho + \kappa_{\mathcal{R}}} \left(1 - \frac{\bar{\mathcal{R}}}{\mathcal{R}_t} \right) \right) = \phi_0 + \phi_{\mathcal{R}} \frac{1}{\mathcal{R}_t}, \quad (18)$$

where $\phi_0 = 1/(\rho + \kappa_{\mathcal{R}})$ and $\phi_{\mathcal{R}} = \bar{\mathcal{R}}\phi_0\kappa_{\mathcal{R}}/\rho$. The instantaneous return of the market portfolio including dividends is

$$dR_t \equiv \frac{dS_t + Y_t dt}{S_t} = \mu_{R,t} dt + \sigma_{R,\hat{Y},t} dZ_{\hat{Y},t} + \sigma_{R,\eta,t} dZ_{\eta,t}$$

with $\sigma_{R,\hat{Y},t} = \sigma_{\hat{Y}} V_{R,t}$ and

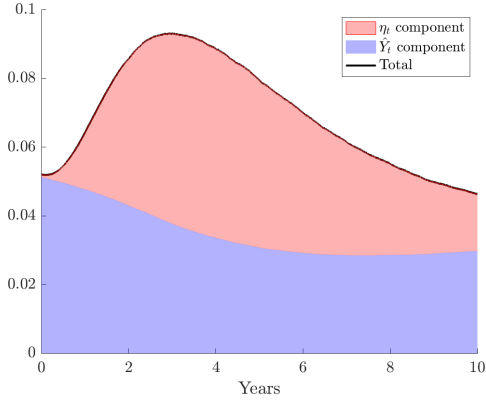
$$V_{R,t} = 1 + \left(\frac{\kappa_{\mathcal{R}} \bar{\mathcal{R}}}{\rho + \kappa_{\mathcal{R}} \bar{\mathcal{R}}} \right) \alpha \left(1 - \frac{\lambda_{\mathcal{R}}}{\mathcal{R}_t} \right). \quad (19)$$

The exposure to shock $Z_{\eta,t}$ is $\sigma_{R,\eta,t} = V_{R,t} \sigma_{\eta} (\lambda - \eta_t)$ if $\omega_t = L$ otherwise is zero. The instantaneous expected return $\mu_{R,t}$, and volatility $\sigma_{R,t}$ are:

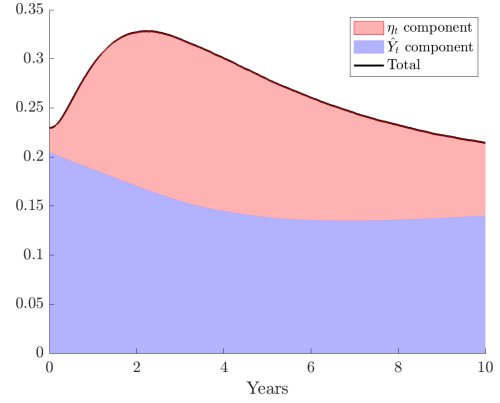
$$\mu_{R,t} = r_t + \theta_{\hat{Y},t} \sigma_{\hat{Y}} V_{R,t} + \hat{\theta}_{\eta,t} \sigma_{\eta} \eta_t (\lambda - \eta_t) V_{R,t}, \quad (20)$$

$$\sigma_{R,t} = V_{R,t} \sqrt{\sigma_{\hat{Y}}^2 + \sigma_{\eta}^2 (\lambda - \eta_t)^2}. \quad (21)$$

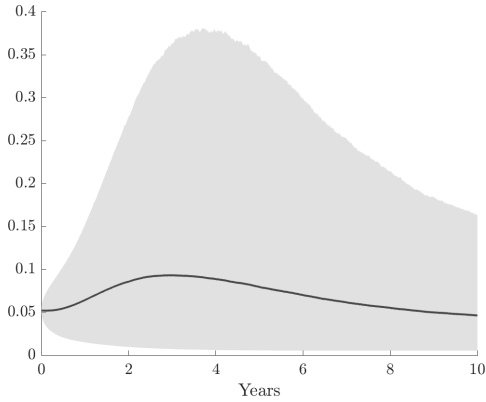
The price-dividend ratio, ϕ_t , strictly decreases as the level of risk aversion, \mathcal{R}_t , increases. Although the volatility of ϕ_t increases with awareness of a new source of risk and exhibits a hump-shaped pattern, its level does not reflect the U-shaped pattern of the output because the conditional expectation of risk aversion does not. However, in the following section, the crisis driver, x_t , directly influences the long-term mean of risk aversion. This results in a



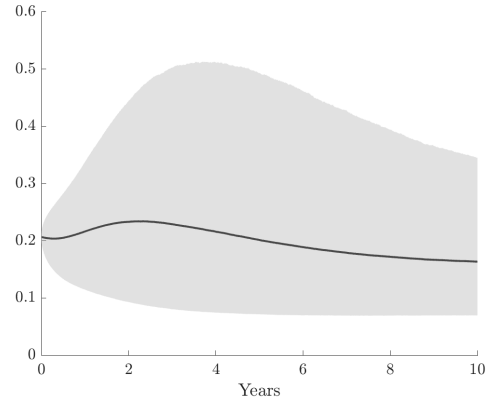
(a) Risk premium



(b) Return volatility



(c) Risk premium with bands



(d) Return volatility with bands

Figure 11. Equilibrium risk premium and return volatility. The figure shows the decomposition of the equilibrium risk premium (Panel (a)) and return volatility (Panel (b)) into the two components driven by output (blue) and η_t risk (orange). Panel (c) and (d) show the equilibrium risk premium and return volatility with 5-95% confidence bands. Parameters used to create this Figure are the following: $\mu_{\hat{Y}} = 0.0197$, $\sigma_{\hat{Y}} = 0.0254$, $\rho = 0.04$, $\kappa_{\mathcal{R}} = 0.16$, $\lambda = 22$, $\bar{\mathcal{R}} = 34$, $\alpha = 25.125$, $\kappa_1 = 0.5$, $\kappa_2 = 3.4$, $\varepsilon = 0.4$, $\kappa_\eta = 0.2$, $\sigma_\eta = 0.3$ and $\lambda_\eta = 1.01$.

decline in the price–dividend ratio, which adopts a U-shaped pattern during crises.

The left column of Figure 11 shows the stock market risk premium, while the right column depicts stock market volatility. In the first row, the black solid line represents the overall stock market risk premium (left plot) and volatility (right plot). The blue area highlights the contribution of the normal risk source $Z_{\hat{Y}}$, while the red line shows the impact of the new risk source Z_{η} . Both the risk premium and volatility follow a hump-shaped pattern, consistent with the data. The second row incorporates 5–95% confidence bands, emphasizing their right-skewed distributions, where the stock market risk premium and volatility more than double in the right tail.

C. Asset pricing with risk aversion amplified during crises

Habit-forming preferences imply that agents become more risk-averse as consumption declines. In the previous section, following Menzly, Santos, and Veronesi (2004), we assumed that risk aversion, \mathcal{R}_t , is locally, perfectly negatively correlated with consumption growth and converges towards a constant long-run mean $\bar{\mathcal{R}}$. However, empirical evidence shows that the price-dividend ratio dips during crises, a pattern not captured by our previous model. To account for this, we now allow agent risk aversion to further increase during crises, leading to a U-shaped pattern in the price-dividend ratio. Specifically, we generalize the previous setup by replacing $\bar{\mathcal{R}}$ in Equation (8) with a time-dependent $\bar{\mathcal{R}}_t$, determined by the consumption crisis driver x_t . Specifically,

$$\bar{\mathcal{R}}_t = \bar{\mathcal{R}} + b(1 - x_t), \quad (22)$$

where $b \geq 0$. Thus, whenever x_t drops below one, the anticipated path of \mathcal{R}_t increases, amplifying the effects of bad consumption shocks on asset prices during crises. In contrast, when the economy recovers and x_t increases to one, risk aversion reverts more rapidly to lower levels. The parameter b governs this “crisis amplification”: a larger b implies a stronger

increase (and subsequent fall) in risk aversion, while $b = 0$ recovers the original model with a constant long-run mean. We explore a range of b values (150–300) to illustrate the sensitivity of asset pricing dynamics to crisis amplification. These are chosen to match key moments in asset returns during select crises.

To analyze how the new source of risk affects asset prices under amplified risk aversion, we focus on one crisis period and thus compute prices for $t \in [s, \tau]$. We assume $\tau = \infty$ when $b > 0$ to enable tractable closed-form solutions for the asset-pricing implications under amplified risk aversion. We cannot derive stock prices in closed form as in Section III. *B.a* due to the complexity of future distributions of entry and exit times. By assuming agents focus only on current crises and setting $\tau = \infty$, we achieve closed-form solutions for equilibrium conditions of the price-dividend ratio and return dynamics. The next proposition presents the market prices of risk, the risk-free rate, and the price-dividend ratio. It shows that, aside from the price-dividend ratio and the habit-driven component in the risk-free rate, these expressions align with Proposition 1. However, dynamics differ due to changes in risk aversion \mathcal{R}_t , leading to more pronounced hump-shaped patterns in stock market risk premia and volatilities, as illustrated in Figure 13.

Proposition 3: *In equilibrium the risk-free rate, r_t , is*

$$r_t = r^{\log} + r_t^{\text{amp.RA}} + r_t^{\text{crisis}} \quad (23)$$

with r^{\log} and r_t^{crisis} given in Proposition 1. The amplified habit-driven component is

$$r_t^{\text{amp.RA}} = \kappa_{\mathcal{R}} \left(1 - \frac{\bar{\mathcal{R}}_t}{\mathcal{R}_t} \right) - \alpha \left(1 - \frac{\lambda_{\mathcal{R}}}{\mathcal{R}_t} \right) \sigma_{\hat{Y}}^2. \quad (24)$$

The expression for the market prices of risks $\theta_{\hat{Y},t}$ and $\theta_{\eta,t}$ are given in Equations (14) and (15) of Proposition 1, respectively. The price-dividend ratio is

$$\phi_t = \phi_0 + \phi_{\mathcal{R}} \frac{1}{\mathcal{R}_t} + \phi_{\mathcal{R}}^{\text{amp.RA}}(t) \frac{1}{\mathcal{R}_t}, \quad (25)$$

where $\phi_0 = 1/(\rho + \kappa_{\mathcal{R}})$ and $\phi_{\mathcal{R}} = \bar{\mathcal{R}}\phi_0\kappa_{\mathcal{R}}/\rho$ is as in Proposition 2. The new crisis term due to amplified risk aversion is $\phi_{\mathcal{R}}^{amp.RA}(t)/\mathcal{R}$ with

$$\phi_{\mathcal{R}}^{amp.RA}(t) = b\kappa_{\mathcal{R}}\phi_0 \left(\frac{e^{-\kappa_1(t-s)}}{\rho + \kappa_1} - \frac{e^{-\kappa_2(t-s)}}{\rho + \kappa_2} \right) \varepsilon. \quad (26)$$

Proposition 3 highlights the impact of heightened risk aversion on the price-dividend (PD) ratio during crises. In this framework, agents' risk aversion increases when a crisis unfolds, leading to a lower inverse surplus consumption ratio. As a result, the PD ratio is influenced both by the direct effect of the crisis driver η_t on output and by the amplified sensitivity of risk aversion. The proposition explicitly accounts for this through the additional term driven by the crisis $\phi_{\mathcal{R}}^{amp.RA}(t)/\mathcal{R}_t$, which captures how shifts in risk aversion dynamically alter asset prices.

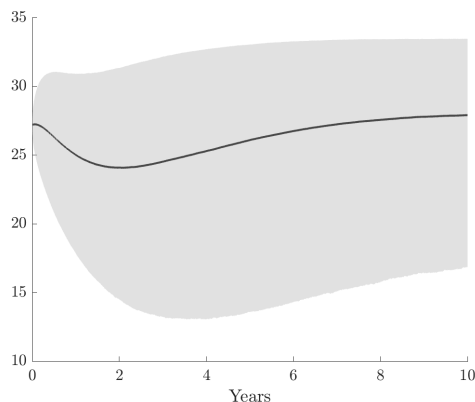


Figure 12. Price-dividend ratio. The figure shows the equilibrium price-dividend ratio in the model with amplified risk aversion. Parameters used to create this Figure are the following: $\mu_{\hat{Y}} = 0.0197$, $\sigma_{\hat{Y}} = 0.0254$, $\rho = 0.04$, $\kappa_{\mathcal{R}} = 0.16$, $\lambda = 22$, $\bar{\mathcal{R}} = 34$, $\alpha = 25.125$, $\kappa_1 = 0.5$, $\kappa_2 = 3.4$, $\varepsilon = 0.4$, $\kappa_{\eta} = 0.2$, $\sigma_{\eta} = 0.3$ and $\lambda_{\eta} = 1.01$. The parameter b is set to 150.

Figure 12 illustrates this mechanism, showing that the PD ratio declines sharply at the onset of a crisis, forming a U-shaped trajectory over time. This pattern emerges as heightened risk aversion initially compresses valuations, pushing the PD ratio downward, before gradually recovering as risk aversion subsides. Unlike standard asset-pricing models where crises primarily affect output without significantly altering risk premia dynamics, this model explains why fundamentals and asset prices exhibit stronger comovement during

downturns. The inclusion of amplified risk aversion effects in the PD ratio provides a possible rationalization for the observed empirical pattern, where valuation ratios fall during crises before rebounding in line with improving economic conditions.

Proposition 4: *The mean and volatility of the instantaneous return including dividends of the market portfolio with price $S_t = \phi_t Y_t$ are*

$$\hat{\mu}_{R,t} = r_t + (\sigma_{\hat{Y}}^2 + \sigma_{\eta}^2 (\lambda - \eta_t)^2) \left(1 + \alpha \left(1 - \frac{\lambda}{\mathcal{R}_t}\right)\right) \left(1 + \frac{\phi_t - \phi_0}{\phi_t \mathcal{R}_t} \alpha \left(1 - \frac{\lambda}{\mathcal{R}_t}\right)\right) \quad (27)$$

$$\sigma_{R,t} = \left(1 + \frac{\phi_t - \phi_0}{\phi_t \mathcal{R}_t} \alpha \left(1 - \frac{\lambda}{\mathcal{R}_t}\right)\right) \sqrt{\sigma_{\hat{Y}}^2 + \sigma_{\eta}^2 (\lambda - \eta_t)^2}. \quad (28)$$

In Figure 13, the black solid line in the left plot represents the stock market risk premium, while the right plot depicts stock market volatility over time since the crisis began at date zero. The blue area indicates the contribution from the Brownian shock $Z_{\hat{Y}}$, and the red area represents the contribution from the new risk source, captured by the Brownian shock Z_{η} . Unlike the previous model, there is a hump-shaped pattern in the normal risk contribution due to increased risk aversion during crises, with additional amplification from the new risk source. Overall, the figure effectively illustrates the hump-shaped patterns in stock market risk premium and volatility during the onset of a crisis, aligning with empirical data.

IV. Data

In this section, we describe the datasets used to analyze aggregate output, consumption, and asset prices. Our analysis spans multiple dimensions, including long-term historical trends, crisis versus non-crisis periods, and sub-samples before and after the 1990s.

A. Aggregate output and consumption

We use quarterly real GDP per capita data and monthly real industrial production from FRED, along with U.S. personal consumption expenditures from the Bureau of Economic

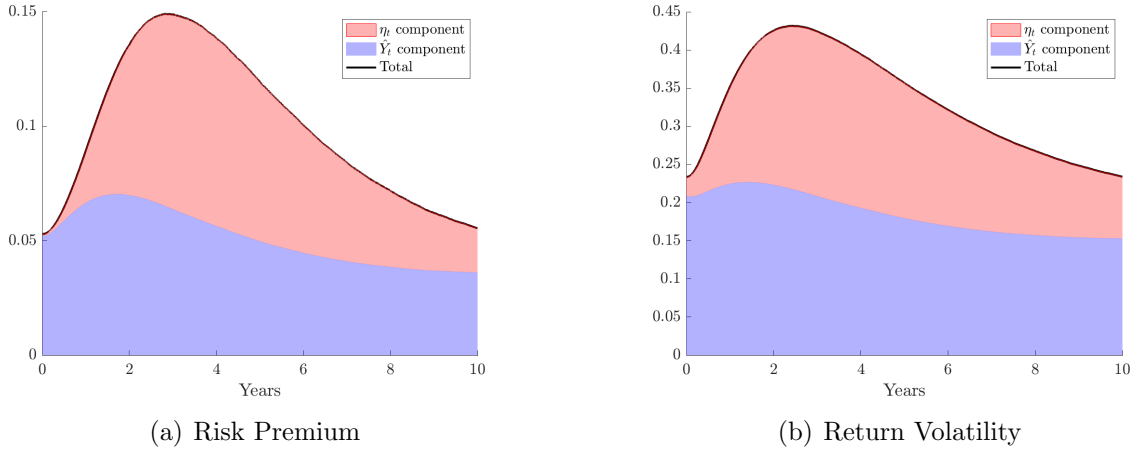


Figure 13. Risk premia and return volatility with risk aversion amplified during crises. The figure shows the decomposition of the equilibrium risk premium (Panel (a)) and return volatility (Panel (b)) into the two components driven by the ‘normal’ output (blue) and η_t risk (orange) in the model described in Section III.C. Parameters used to create this Figure are the following: $\mu_{\hat{Y}} = 0.0197$, $\sigma_{\hat{Y}} = 0.0254$, $\rho = 0.04$, $\kappa_{\mathcal{R}} = 0.16$, $\lambda = 22$, $\bar{\mathcal{R}} = 34$, $\alpha = 25.125$, $\kappa_1 = 0.5$, $\kappa_2 = 3.4$, $\varepsilon = 0.4$, $\kappa_{\eta} = 0.2$, $\sigma_{\eta} = 0.3$ and $\lambda_{\eta} = 1.01$. The parameter b is set to 150.

Analysis. We measure year-on-year (Y-o-Y) and quarter-on-quarter (Q-on-Q) log growth rates of real GDP per capita and real personal consumption expenditures per capita over the entire sample period (January 1947 to June 2024). Additionally, we analyze these growth rates in sub-samples: pre-1990s, post-1990s, during crisis periods, and during normal times. Table I summarizes the results.

Real GDP grew at an average annualized rate of 1.973% (Y-o-Y) and 1.954% (Q-on-Q) over the entire sample period, while real consumption increased by 2.09% (Y-o-Y). In crisis periods, output growth drops to -0.195% (Y-o-Y) or increases only modestly by 0.466% (Q-on-Q), and consumption growth slows to 0.471% (Y-o-Y) and 1.067% (Q-on-Q). During normal times, output grows at a robust rate of 2.964% (Y-o-Y), with similar consumption growth.

Volatility rises significantly during crises. The volatility ratios, calculated as the ratio of standard deviations during crises to those during normal times, range from 1.36 (Y-o-Y) to 2.41 (Q-on-Q) for GDP growth and from 1.40 (Y-on-Y) to 2.07 (Q-on-Q) for consumption growth.

	GDP growth		Consumption growth	
	Y-on-Y	Q-on-Q	Y-on-Y	Q-on-Q
Entire sample: 1947 - 2024	1.973% (2.535%)	1.954% (2.234%)	2.090% (2.206%)	2.089% (2.171%)
Pre-1990s	2.304% (2.868%)	2.257% (2.204%)	2.325% (2.197%)	2.313% (1.911%)
Post 1990s	1.570% (2.008%)	1.578% (2.259%)	1.804% (2.200%)	1.812% (2.447%)
During crises	-0.195% (2.504%)	0.466% (3.330%)	0.471% (2.145%)	1.067% (3.127%)
During normal times	2.964% (1.835%)	2.964% (1.385%)	2.750% (1.537%)	2.527% (1.509%)
Crisis-to-non-crisis volatility ratio	1.3647	2.4047	1.3954	2.0713

Table I Quarterly GDP and Consumption Growth Data. This table shows annualized growth rates and standard deviations for quarterly real gross domestic product (GDP) and quarterly consumption per capita. Y-on-Y indicates year-on-year, Q-on-Q means quarter-on-quarter, both annualized, using data from January 1947 to June 2024. Real gross domestic product per capita [A939RX0Q048SBEA] and real personal consumption expenditures per capita [A794RX0Q048SBEA] were retrieved from FRED, Federal Reserve Bank of St. Louis, on October 3, 2024.

B. Asset prices

We obtain market return data from 1929 to 2019 from Kenneth French’s website and the Center for Research in Security Prices (CRSP) Index Stock File. Market excess returns and the annual risk-free rate are adjusted for inflation using the Personal Consumption Expenditures (PCE) deflator. In addition, we incorporate the VIX, a widely used measure of stock market return volatility. VIX data is sourced from FRED and spans the period from 1990 to 2021, providing insights into market uncertainty during crises.

As a measure of stock market value, we use the cyclically adjusted price-to-earnings (CAPE) ratio introduced by Campbell and Shiller (1998), which smooths corporate profit fluctuations over business cycles. CAPE data, spanning 1871 to 2023, is collected from Robert Shiller’s website. As a proxy for stock market risk premia, we use two measures: (i) the stochastic volatility-derived risk premia index by Marfè and Pénasse (2024), covering the period from 1874 to 2018; and (ii) the lower bound on market risk premia developed by

Martin (2017), covering the period from 1996 to 2012.

V. Matching output dynamics during the GFC period

We calibrate the model to match the GDP dynamics observed during the Global Financial Crisis (GFC), covering the period from April 2008 to January 2013. We estimate parameters driving the crisis trigger η_t and the crisis driver x_t , which determine output during a crisis. Importantly, we avoid using asset-pricing data in the estimation process, allowing us to test the model's capability to generate meaningful asset-pricing insights without explicit calibration to asset prices.

We estimate the model parameters by comparing mean trajectories of simulated output with observed data. We design the objective function to minimize a weighted combination of two error components. The first term measures the squared difference between the observed output and the simulated mean output, summed across all quarters. The second term penalizes deviations between the simulated and observed crisis-to-non-crisis output volatility ratios.

$$\min_{\theta} \left\{ w \sum_{t=1}^T [\bar{Y}_t^{sim}(\theta) - Y_t^{obs}]^2 + (1-w) \left[\left(\frac{\sigma_Y^{crisis}}{\sigma_Y^{non-crisis}}(\theta) \right)^{sim} - \left(\frac{\sigma_Y^{crisis}}{\sigma_Y^{non-crisis}} \right)^{obs} \right]^2 \right\}, \quad (29)$$

where $\bar{Y}_t^{sim}(\theta) = \sum_{i=1}^N Y_t^{sim}(\theta)$.

The simulated volatility ratio is computed by

$$\left(\frac{\sigma_Y^{crisis}}{\sigma_Y^{non-crisis}}(\theta) \right)^{sim} = \frac{\sigma_{\hat{Y}} + \sigma_{\eta}(\lambda - \bar{\eta})}{\sigma_{\hat{Y}}}, \quad (30)$$

where $\bar{\eta}$, $\bar{\eta} = \sum_{i=1}^N \sum_{t=1}^T \eta_t^i$, is the mean simulated η value across all simulations and all quarterly periods. The observed crisis-to-non-crisis volatility ratio we match equals 1.8847 (the average Y-on-Y and Q-on-Q crisis-to-non-crisis volatility ratios for real GDP growth, see Table I). By incorporating both terms, we ensure that the model matches both the first and second

moments of observed output data.

We estimate parameters using particle swarm optimization, a global search algorithm well-suited for complex, non-convex optimization problems.⁸ This algorithm iteratively adjusts parameters from the vector θ to minimize the weighted error while respecting lower and upper bounds. The calibrated parameters include the reversion speeds of the crisis driver x_t (κ_1 and κ_2), the volatility and reversion speed of the crisis impact η_t (σ_η and κ_η), and the magnitude of the crisis shock (ε).

We simulate 10,000 paths of 20 quarters to match the length of the GFC period. We set the weight parameter w to 0.9. Our results are robust when choosing alternative values of w . We choose $w = 0.9$ to make matching both moments of crisis output relevant when matching the observed GFC crisis output dynamics. If we set w to 1, the parameter σ_η , and thus the second moment of output observed during crises, would not be well-identified. We define the following lower and upper bounds for θ :

$$\theta_{min} = [0.45, 1, 0.1, 0.01, 0.01],$$

$$\theta_{max} = [0.6, 5, 2, 5, 5],$$

and starting values to be

$$\theta_0 = [0.5, 4, 0.5, 0.4, 0.4].$$

Lower and upper bounds for κ_1 and κ_2 are set to ensure that the process x_t converges to one within a reasonable amount of time and does not stay below one indefinitely.

The remaining model parameters are set to match the unconditional GDP growth rate (Y-on-Y) and its volatility from our sample period (see Panel A in Table I). Preference parameters are the same as in Menzly, Santos, and Veronesi (2004) (see Panel B in Table I).

Table II reports the estimated parameters. These estimates yield a simulated crisis-to-

⁸We use the Matlab function *particleswarm*, which runs a bound-constrained optimization using particle swarm optimization.

non-crisis volatility ratio of 1.8911, closely matching the data counterpart with a difference of 0.064 units. The combination of the estimated κ parameters and the ε shock generates a severity and duration of the crisis that are quantitatively consistent with observed data.

This table presents the parameters governing aggregate output dynamics during normal times (Panel A) and agent preferences (Panel B). The parameters in Panel A are estimated using real GDP growth data from January 1947 to June 2024 (full sample), as detailed in Table I. Preference parameters in Panel B are based on Menzly, Santos, and Veronesi (2004), except for α , which is set to a lower value of 25.125 to account for the newly introduced crisis component that increases output volatility.

Table II Parameters describing the Aggregate Economy and Preferences. This table presents the parameters governing aggregate output dynamics during normal times (Panel A) and agent preferences (Panel B). The parameters in Panel A are estimated using real GDP growth data from January 1947 to June 2024 (full sample), as detailed in Table I. Preference parameters in Panel B are based on Menzly, Santos, and Veronesi (2004), except for α , which is set to a lower value of 25.125 to account for the newly introduced crisis component that increases output volatility.

Panel A: Real GDP growth (1947-2024)	
μ_Y	1.973%
σ_Y	2.535%
Panel B: Parameters from Menzly, Santos, and Veronesi (2004)	
ρ	0.04
λ	20
κ_R	0.16
\bar{R}	34
α	25.125

Figure 14 illustrates the observed levels of output (black solid line) alongside the fitted output from the estimation (blue dash-dotted line). The Global Financial Crisis is notable for its particularly sluggish recovery, which stands out compared to other economic downturns. Our model, however, implies a slightly faster reversion of output back to its pre-crisis level and a smaller total dip in output at the crisis trough. Despite these differences, the model

Table III Estimated Parameters for the GFC period. This table presents the estimated parameters used to match the model with output dynamics observed during the GFC period. These parameters from the crisis driver x_t and crisis impact η_t processes determine how output evolves during each crisis.

Parameter θ_i	Estimated Value
κ_1	0.5316
κ_2	3.4321
κ_η	0.2231
σ_η	0.3104
ε	0.4310

captures the dynamics of output during this specific crisis period well, as reflected in the estimated parameters.

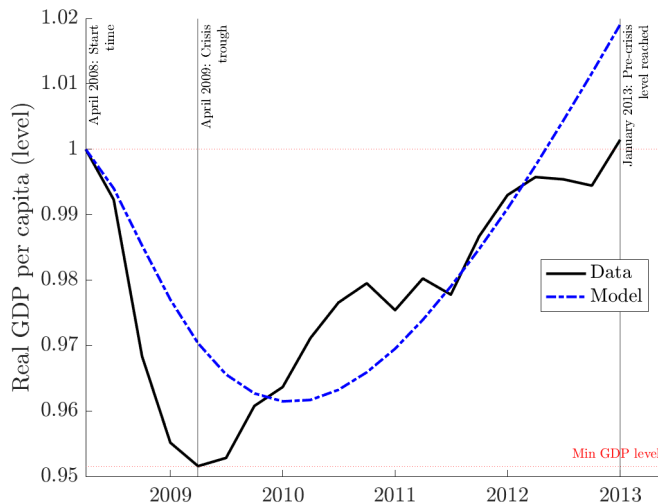


Figure 14. Matching GDP dynamics observed during the GFC period. This figure shows the quarterly level of U.S. real GDP per capita, indexed to 1 in April 2008 (black line). The blue dash-dotted line represents the fitted output data, obtained from our estimation.

We use the estimated model parameters to predict how asset prices would behave during the Global Financial Crisis period and compare these predictions with empirical data in Figure 15. We examine risk premia from Marfè and Pénasse (2024) and the lower bound of the equity premium from Martin (2017) in Panel (a); the Shiller’s CAPE ratio in Panel (b); and VIX and realized volatility, calculated as the annualized standard deviation of the total

daily squared returns (evaluated monthly), in Panel (c).

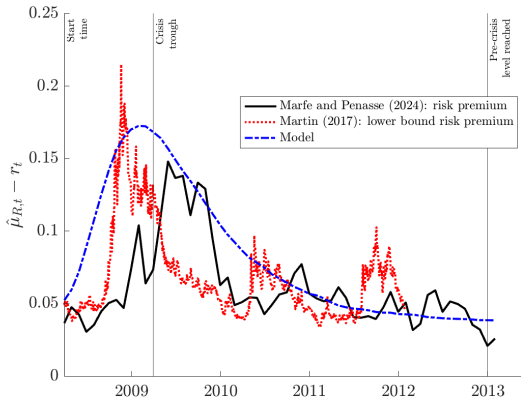
The asset-pricing predictions generated by our model align well with observed data, both in terms of the dynamics and levels. Specifically, the implied risk premium from Marfè and Pénasse (2024) and the lower bound of the equity premium from Martin (2017) both exhibit a distinct hump-shaped trend that matches the predictions of the model. Realized volatility shows a marked hump shape during the early stages of the GFC. Our model can quantitatively match the size of the increase in risk premia as well as the intensity of realized volatility, which peaks at 40% during the deepest point of the crisis.

Note that in our model, the increase in the risk premia and return volatility is linked to the increase in output volatility. Although it is difficult to measure the output volatility at a high enough frequency during a recession, we plot the squared growth of industrial production in Panel (d) of Figure 15. Here we see the same pattern: a hump-shaped volatility. This pattern is consistent with our model and is an important driver of the joint dynamics of risk premia and return volatility.

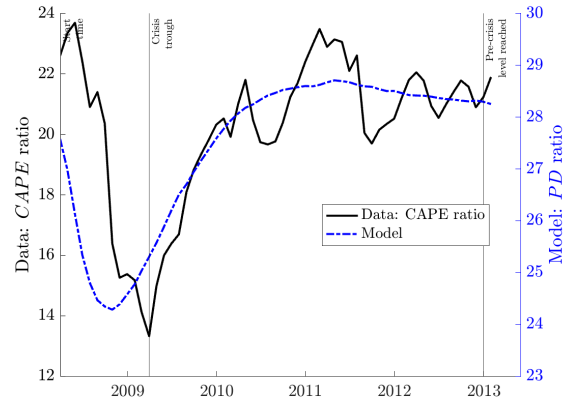
Lastly, we analyze the model’s sensitivity to parameter b , which governs agents’ responsiveness to the crisis variable x_t . When $b = 0$, crises do not affect agent average risk aversion, whereas higher b values strengthen the impact of crises on asset prices by amplifying agent risk aversion. Figure 16 displays model predictions for the GFC period across different values of b . Even with $b = 0$, risk premia and return volatility exhibit a hump-shaped pattern, which becomes more pronounced as b increases. Notably, the decline in the price-dividend ratio emerges only when $b > 0$, driven by heightened risk aversion during crises.

A. Other crisis periods

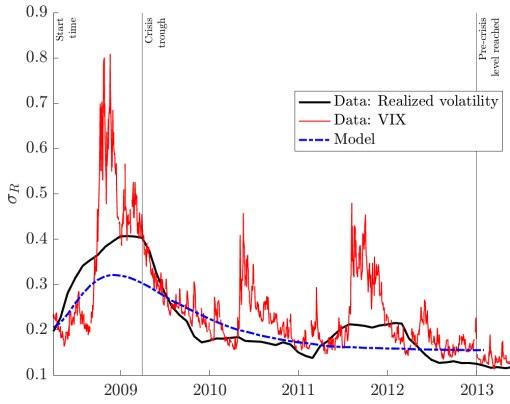
In Appendix B, we replicate the estimation for the remaining eight NBER crises recorded since 1947. Specifically, we match the output process observed during the individual crisis episodes and then use the estimated ‘crisis’ parameters to study how asset prices would evolve. We compare the model-implied asset pricing moments with data. Our model captures



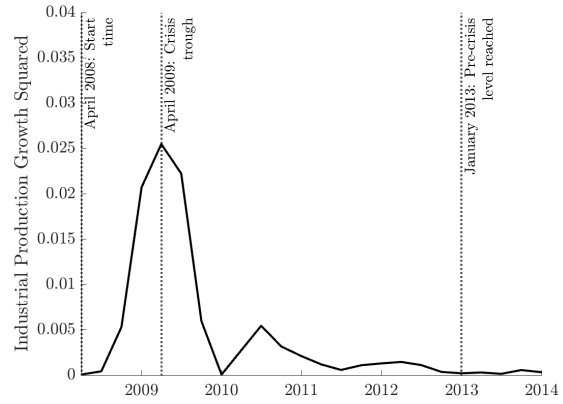
(a) Risk Premium



(b) Price-dividend ratio



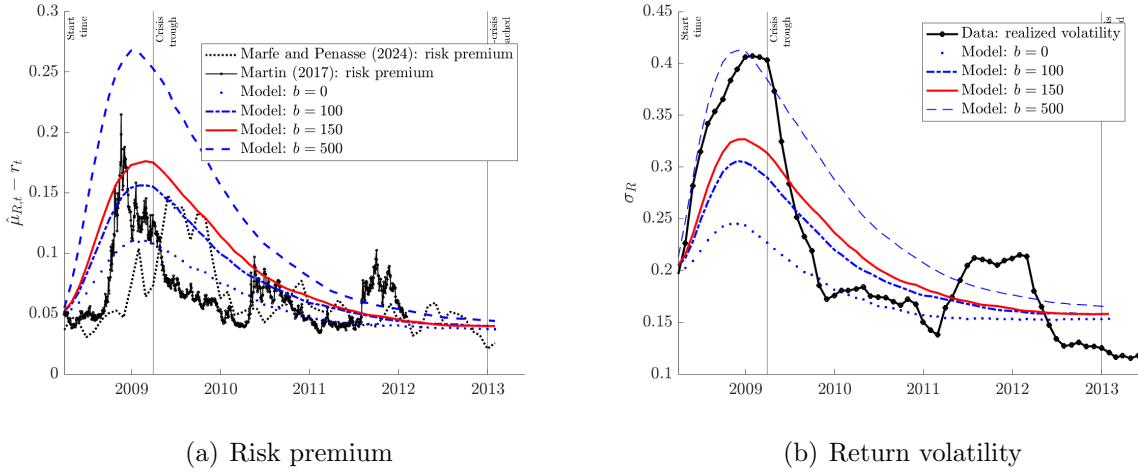
(c) Return volatility



(d) Industrial Production Variance

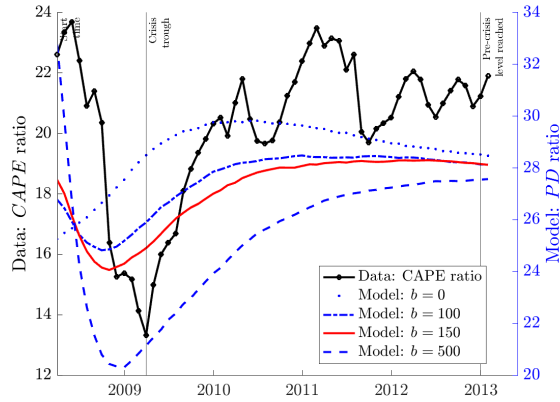
Figure 15. GFC period – Implied asset-pricing moments. This figure compares the mean simulated model predictions (blue dashed-dotted lines) with equity risk premia: the Marfè and Pénasse (2024) index (red dotted line) and Martin (2017)’s lower bound (black solid line) in Panel (a); the CAPE ratio (black solid line) in Panel (b); and monthly realized volatility using daily returns (black solid line) and the VIX (red line) in Panel (c). Panel (d) plots the squared industrial production growth. Model predictions are generated with $b = 150$.

key features of asset pricing dynamics during several other recessions, with varying degrees of precision depending on the severity and duration of the crisis. Figures in Appendix B show that our model produces realistic paths of the levels of price-dividend ratio, risk premium, and return volatility, across numerous crisis events.



(a) Risk premium

(b) Return volatility



(c) Price-dividend ratio

Figure 16. GFC period – Sensitivity analysis for parameter b . This figure presents the mean simulated model predictions (depicted by blue and red lines) for different values of parameter b , that is, 0, 100, 150 (in red), and 500 — alongside empirical observations (shown in black lines). Specifically, we compare equity risk premia, measured using the Marfè and Pénasse (2024) index derived from stochastic volatility and the lower bound on market risk premia developed by Martin (2017) in Panel (a); return volatility measured using monthly realized volatility in Panel (b); and the price-dividend ratio measured using the Campbell-Shiller CAPE ratio in Panel (c), with model predictions.

VI. Conclusion

In this paper, we present a novel equilibrium model that captures the dynamics of asset prices during crises triggered by the emergence of new risks. Our model incorporates two key empirical observations: the delayed decline in output following the introduction of new risks, and the subsequent recovery phase characterized by abnormally high positive growth. By

introducing a new stochastic process, η , we are able to model the gradual decline in output leading up to a crisis as well as the accelerated growth during the recovery period.

Our model matches asset-pricing dynamics during crises. Specifically, we demonstrate that asset prices exhibit a delayed response to new risks, with expected returns displaying a hump-shaped pattern as the crisis unfolds. This dynamic results in a delayed reaction of asset prices to news about future economic activity, challenging traditional asset-pricing models that predict immediate market reactions.

By calibrating our model to output data and excluding asset-pricing moments, we test its ability to replicate asset price dynamics during crises. The successful application of our model to the Global Financial Crisis (GFC) and other NBER recessions underscores its general applicability and effectiveness in explaining how the awareness of new priced risks affects the real economy and financial markets.

Our approach fills a gap in the literature by directly linking asset price behavior to output dynamics during crises. It provides a rational explanation for the delayed reaction of asset prices and their hump-shaped patterns, highlighting the significant role of new risks in shaping asset pricing dynamics. This has important implications for investors and policymakers, as understanding the timing and magnitude of asset price responses to new risks can inform investment strategies and policy decisions aimed at mitigating the impact of economic downturns.

REFERENCES

- Ai, H., 2010, “Information Quality and Long-Run Risk: Asset Pricing Implications,” *The Journal of Finance*, 65(4), 1333–1367.
- Ai, H., and R. Bansal, 2018, “Risk Preferences and the Macroeconomic Announcement Premium,” *Econometrica*, 86(4), 1383–1430.
- Ai, H., and A. Bhandari, 2021, “Asset pricing with endogenously uninsurable tail risk,” *Econometrica*, 89(3), 1471–1505.
- Bansal, R., and A. Yaron, 2004, “Risks for the Long Run: A Potential Resolution of Asset Pricing Puzzles,” *The Journal of Finance*, 59, 1481–1509.
- Barro, R. J., and J. Ursúa, 2008, “Consumption disasters in the twentieth century,” *American Economic Review*, 98(2), 58–63.
- Basu, S., G. Candian, R. Chahrour, and R. Valchev, 2021, “Risky business cycles,” Working paper, National Bureau of Economic Research.
- Beaudry, P., and F. Portier, 2006, “Stock prices, news, and economic fluctuations,” *American Economic Review*, 96(4), 1293–1307.
- Beeler, J., and J. Y. Campbell, 2012, “The Long-Run Risks Model and Aggregate Asset Prices: An Empirical Assessment,” *Critical Finance Review*, 1(1), 141–182.
- Blanchard, O. J., 1985, “Debt, deficits, and finite horizons,” *Journal of Political Economy*, 93(2), 223–247.
- Bordo, M. D., and J. G. Haubrich, 2017, “Deep recessions, fast recoveries, and financial crises: Evidence from the American record,” *Economic Inquiry*, 55(1), 527–541.
- Brunnermeier, M., D. Palia, K. A. Sastry, and C. A. Sims, 2021, “Feedbacks: financial markets and economic activity,” *American Economic Review*, 111(6), 1845–1879.

- Campbell, J. Y., and J. H. Cochrane, 1999, “By Force of Habit: A Consumption Based Explanation of Aggregate Stock Market Behavior,” *Journal of Political Economy*, 107, 205–251.
- Campbell, J. Y., and R. J. Shiller, 1998, “Valuation ratios and the long-run stock market outlook.” *Journal of Portfolio Management*, 24(2), 11–26.
- Christiano, L. J., M. Eichenbaum, and C. L. Evans, 2005, “Nominal rigidities and the dynamic effects of a shock to monetary policy,” *Journal of Political Economy*, 113(1), 1–45.
- Fernald, J. G., 2015, “Productivity and Potential Output before, during, and after the Great Recession,” *NBER Macroeconomics Annual*, 29(1), 1–51.
- Gârleanu, N., and S. Panageas, 2015, “Young, old, conservative, and bold: The implications of heterogeneity and finite lives for asset pricing,” *Journal of Political Economy*, 123(3), 670–685.
- Ghaderi, M., M. Kilic, and S. B. Seo, 2022, “Learning, slowly unfolding disasters, and asset prices,” *Journal of Financial Economics*, 143(1), 527–549.
- Gourio, F., 2012, “Disaster risk and business cycles,” *American Economic Review*, 102(6), 2734–2766.
- Hamilton, J. D., 1989, “A new approach to the economic analysis of nonstationary time series and the business cycle,” *Econometrica: Journal of the Econometric Society*, 357–384.
- Hasler, M., and R. Marfè, 2016, “Disaster recovery and the term structure of dividend strips,” *Journal of Financial Economics*, 122(1), 116–134.
- Illeditsch, P., 2011, “Ambiguous Information, Portfolio Inertia, and Excess Volatility,” *The Journal of Finance*, 66(6), 2213–2247.

- Illeditsch, P., 2021, “Information Inertia,” *The Journal of Finance*, 76(1), 443–479.
- Jordà, Ò., M. Schularick, and A. M. Taylor, 2011, “Financial crises, credit booms, and external imbalances: 140 years of lessons,” *IMF Economic Review*, 59(2), 340–378.
- Kim, C.-J., J. Morley, and J. Piger, 2005, “Nonlinearity and the permanent effects of recessions,” *Journal of Applied Econometrics*, 20(2), 291–309.
- Kroencke, T. A., 2022, “Recessions and the stock market,” *Journal of Monetary Economics*, 131, 61–77.
- Lucas, R. E., 1978, “Asset Prices in an Exchange Economy,” *Econometrica*, 46(6), 1429–1445.
- Lustig, H., and A. Verdelhan, 2012, “Business cycle variation in the risk-return trade-off,” *Journal of Monetary Economics*, 59, S35–S49.
- Marfè, R., and J. Pénasse, 2024, “Measuring macroeconomic tail risk,” *Journal of Financial Economics*, 156, 103838.
- Martin, I., 2017, “What is the Expected Return on the Market?” *The Quarterly Journal of Economics*, 132(1), 367–433.
- Menzly, L., T. Santos, and P. Veronesi, 2004, “Understanding predictability,” *Journal of Political Economy*, 112(1), 1–47.
- Morley, J., and J. Piger, 2012, “The asymmetric business cycle,” *Review of Economics and Statistics*, 94(1), 208–221.
- Muir, T., 2017, “Financial crises and risk premia,” *The Quarterly Journal of Economics*, 132(2), 765–809.

- Nakamura, E., J. Steinsson, R. Barro, and J. Ursúa, 2013, “Crises and recoveries in an empirical model of consumption disasters,” *American Economic Journal: Macroeconomics*, 5(3), 35–74.
- Neftci, S. N., 1984, “Are economic time series asymmetric over the business cycle?” *Journal of Political Economy*, 92(2), 307–328.
- Reinhart, C. M., and K. S. Rogoff, 2009, *This time is different: Eight centuries of financial folly*, Princeton University press.
- Smets, F., and R. Wouters, 2007, “Shocks and frictions in US business cycles: A Bayesian DSGE approach,” *American Economic Review*, 97(3), 586–606.
- Tsai, J., and J. A. Wachter, 2015, “Disaster risk and its implications for asset pricing,” *Annual Review of Financial Economics*, 7(1), 219–252.
- Wachter, J. A., 2013, “Can time-varying risk of rare disasters explain aggregate stock market volatility?” *The Journal of Finance*, 68(3), 987–1035.

Appendix A. Proofs

In this Section, we provide comprehensive proofs for the propositions presented in the main text of Section III. Before we provide proofs for the propositions, we present the output and risk aversion dynamics in a normal and a crisis regime. Specifically, applying Itô's lemma to $Y_t = \hat{Y}_t \eta_t$ leads to the following output dynamics.

$$\frac{dY_t}{Y_t} = \begin{cases} (\mu_{\hat{Y}} + \kappa_{\eta} (x_t/\eta_t - 1)) dt + \sigma_{\hat{Y}} dZ_{\hat{Y},t} + \sigma_{\eta} (\lambda - \eta_t) dZ_{\eta,t} & \text{if } \omega_t = L \\ \mu_{\hat{Y}} dt + \sigma_{\hat{Y}} dZ_{\hat{Y},t} & \text{if } \omega_t = H \end{cases} \quad (\text{A1})$$

Using Equation (A1) and plugging in the shocks to output in Equation (8) leads to the dynamics of risk aversion \mathcal{R}_t . Specifically,

$$d\mathcal{R}_t = \kappa_{\mathcal{R}} (\bar{\mathcal{R}}_t - \mathcal{R}_t) dt - \alpha (\mathcal{R}_t - \lambda_{\mathcal{R}}) \begin{cases} \sigma_{\hat{Y}} dZ_{\hat{Y},t} + \sigma_{\eta} (\lambda - \eta_t) dZ_{\eta,t} & \text{if } \omega_t = L \\ \sigma_{\hat{Y}} dZ_{\hat{Y},t} & \text{if } \omega_t = H \end{cases} \quad (\text{A2})$$

where $\bar{\mathcal{R}}_t = \bar{\mathcal{R}} + b(1 - x_t)$ with $b = 0$ in Section III. *B.a* and $b > 0$ in Section III.C.

Proof of Proposition 1. The risk-free rate and the market prices of risk are derived from the dynamics of the SDF, $M_t = e^{-\rho t} \frac{\mathcal{R}_t}{Y_t}$. Suppose that we are in normal times (i.e., $\omega_t = H$). Then applying Itô's lemma to M_t and using Equations (A1) and (A2) leads to

$$\frac{dM_t}{M_t} = - \underbrace{\left(\rho + \mu_{\hat{Y}} - \sigma_{\hat{Y}}^2 + \kappa_{\mathcal{R}} (1 - \bar{\mathcal{R}}/\mathcal{R}_t) - \alpha \left(1 - \frac{\lambda_{\mathcal{R}}}{\mathcal{R}_t} \right) \sigma_{\hat{Y}}^2 \right)}_{= r_t} dt - \underbrace{\sigma_{\hat{Y}} \left(1 + \alpha \left(1 - \frac{\lambda_{\mathcal{R}}}{\mathcal{R}_t} \right) \right)}_{=\theta_{\hat{Y},t}} dZ_{\hat{Y},t}.$$

We know that the risk-free rate and market price of output risk in an economy with i.i.d. output growth and a representative agent (RA) with log utility and time discount rate ρ is equal to $r^{\log} = \rho + \mu_{\hat{Y}} - \sigma_{\hat{Y}}^2$ and $\sigma_{\hat{Y}}$, respectively. Hence, $r_t = r^{\log} + r_t^{\text{habit}}$ with $r_t^{\text{habit}} = \kappa_{\mathcal{R}} (1 - \bar{\mathcal{R}}/\mathcal{R}_t) - \alpha \left(1 - \frac{\lambda_{\mathcal{R}}}{\mathcal{R}_t} \right) \sigma_{\hat{Y}}^2$. Moreover, the habit amplifies the market price of output risk by the factor $\alpha \left(1 - \frac{\lambda_{\mathcal{R}}}{\mathcal{R}_t} \right)$.

Suppose that we are in crisis times (i.e., $\omega_t = L$). Then applying Itô's lemma to M_t and using Equations (A1) and (A2), and the expressions for r^{\log} , r_t^{habit} , and $\theta_{\hat{Y},t}$ from above leads to

$$\begin{aligned} \frac{dM_t}{M_t} = & - \underbrace{\left(r^{\log} + r_t^{\text{habit}} + \kappa_\eta (x_t/\eta_t - 1) - \sigma_\eta^2 (\lambda - \eta_t)^2 - \alpha \left(1 - \frac{\lambda \mathcal{R}}{\mathcal{R}_t} \right) \sigma_\eta^2 (\lambda - \eta_t)^2 \right)}_{=r_t} dt \\ & - \theta_{\hat{Y},t} dZ_{\hat{Y},t} - \underbrace{\left[\sigma_\eta (\lambda - \eta_t) \left(1 + \alpha \left(1 - \frac{\lambda \mathcal{R}}{\mathcal{R}_t} \right) \right) \right]}_{=\theta_{\eta,t}} dZ_{\eta,t}. \end{aligned}$$

The additional term in the risk-free rate is equal to r_t^{crisis} given in Equation (13). \square

Proof of Proposition 2. The market portfolio is a claim on the continuous output stream $S_t = \phi_t Y_t$. The valuation ratio ϕ_t is given in Equation (17). Specifically,

$$\begin{aligned} \phi_t &= \int_t^\infty e^{-\rho(u-t)} \mathbb{E}_t \left[\frac{\mathcal{R}_u}{\mathcal{R}_t} \right] du = \int_t^\infty e^{-\rho(u-t)} \left(\frac{\bar{\mathcal{R}}}{\mathcal{R}_t} + \left(1 - \frac{\bar{\mathcal{R}}}{\mathcal{R}_t} \right) e^{-\kappa_{\mathcal{R}}(u-t)} \right) du \\ &= \frac{\bar{\mathcal{R}}}{\mathcal{R}_t} \int_t^\infty e^{-\rho(u-t)} du + \left(1 - \frac{\bar{\mathcal{R}}}{\mathcal{R}_t} \right) \int_t^\infty e^{-(\rho+\kappa_{\mathcal{R}})(u-t)} du \\ &= \frac{\bar{\mathcal{R}}}{\mathcal{R}_t} \frac{1}{\rho} + \left(1 - \frac{\bar{\mathcal{R}}}{\mathcal{R}_t} \right) \frac{1}{\rho + \kappa_{\mathcal{R}}} = \frac{1}{\rho + \kappa_{\mathcal{R}}} + \frac{\kappa_{\mathcal{R}}/\rho}{\rho + \kappa_{\mathcal{R}}} \frac{\bar{\mathcal{R}}}{\mathcal{R}_t} = \phi_0 + \phi_{\mathcal{R}} \frac{1}{\mathcal{R}_t}, \end{aligned} \tag{A3}$$

where $\phi_0 = \frac{1}{\rho + \kappa_{\mathcal{R}}}$ and $\phi_{\mathcal{R}} = \frac{\kappa_{\mathcal{R}}/\rho}{\rho + \kappa_{\mathcal{R}}} \bar{\mathcal{R}}$. The dynamics of the valuation ratio ϕ_t are

$$\frac{d\phi_t}{\phi_t} = \frac{\phi_{\mathcal{R}}}{\phi_t} d \left(\frac{1}{\mathcal{R}_t} \right) = - \frac{\phi_{\mathcal{R}}}{\phi_t} \frac{d\mathcal{R}_t}{\mathcal{R}_t^2} + \frac{\phi_{\mathcal{R}}}{\phi_t} \frac{(d\mathcal{R}_t)^2}{\mathcal{R}_t^3}. \tag{A4}$$

Determining the stochastic part in normal and crisis times for the valuation ratio leads to

$$\frac{d\phi_t}{\phi_t} = \dots dt + \alpha \frac{\phi_{\mathcal{R}}/\mathcal{R}_t}{\phi_t} \left(1 - \frac{\lambda \mathcal{R}}{\mathcal{R}_t} \right) \begin{cases} \sigma_{\hat{Y}} dZ_{\hat{Y},t} + \sigma_\eta (\lambda - \eta_t) dZ_{\eta,t} & \text{if } \omega_t = L \\ \sigma_{\hat{Y}} dZ_{\hat{Y},t} & \text{if } \omega_t = H \end{cases} \tag{A5}$$

The equilibrium stock price is $S_t = Y_t \phi_t$ and its instantaneous return including dividends is

$$dR_t \equiv \frac{dS_t + Y_t dt}{S_t} = \mu_{R,t} dt + \sigma_{R,\hat{Y},t} dZ_{\hat{Y},t} + \sigma_{R,\eta,t} dZ_{\eta,t}.$$

Suppose $\omega_t = H$, applying Itô's lemma to $S_t = Y_t \phi_t$ leads to

$$\frac{dS_t}{S_t} = \frac{d\hat{Y}_t}{\hat{Y}_t} + \frac{d\phi_t}{\phi_t} + \frac{d\hat{Y}_t}{\hat{Y}_t} \frac{d\phi_t}{\phi_t} = \dots dt + \sigma_{\hat{Y}} dZ_{\hat{Y},t} + \alpha \frac{\phi_{\mathcal{R}}/\mathcal{R}_t}{\phi_t} \left(1 - \frac{\lambda_{\mathcal{R}}}{\mathcal{R}_t}\right) \sigma_{\hat{Y}} dZ_{\hat{Y},t}.$$

Hence, $\sigma_{R,\hat{Y},t} = \sigma_{\hat{Y}} V_{R,t}$ and $\sigma_{R,\eta,t} = 0$ with

$$V_{R,t} = 1 + \alpha \frac{\phi_{\mathcal{R}}/\mathcal{R}_t}{\phi_t} \left(1 - \frac{\lambda_{\mathcal{R}}}{\mathcal{R}_t}\right) = 1 + \alpha \frac{\phi_t - \phi_0}{\phi_t} \left(1 - \frac{\lambda_{\mathcal{R}}}{\mathcal{R}_t}\right) = 1 + \frac{\kappa_{\mathcal{R}} \bar{\mathcal{R}}}{\rho + \kappa_{\mathcal{R}} \bar{\mathcal{R}}} \alpha \left(1 - \frac{\lambda_{\mathcal{R}}}{\mathcal{R}_t}\right). \quad (\text{A6})$$

Suppose $\omega_t = L$, applying Itô's lemma to $S_t = Y_t \phi_t$, using Equation (A6) leads to

$$\frac{dS_t}{S_t} = \frac{dY_t}{Y_t} + \frac{d\phi_t}{\phi_t} + \frac{dY_t}{Y_t} \frac{d\phi_t}{\phi_t} = \dots dt + V_{R,t} \sigma_{\hat{Y}} dZ_{\hat{Y},t} + V_{R,t} \sigma_{\eta} (\lambda - \eta_t) dZ_{\eta,t}.$$

Hence, we have that $\sigma_{R,\hat{Y},t} = \sigma_{\hat{Y}} V_{R,t}$ and $\sigma_{R,\eta,t} = V_{R,t} \sigma_{\eta} (\lambda - \eta_t)$. If $\omega_t = H$, then the instantaneous stock market volatility is $\sigma_{R,t} = \sigma_{\hat{Y}} V_{R,t}$. The Brownian shocks $Z_{\hat{Y},t}$ and $Z_{\eta,t}$ are independent and thus the instantaneous stock market volatility if $\omega_t = L$ is $\sigma_{R,t} = V_{R,t} \sqrt{\sigma_{\hat{Y}}^2 + \sigma_{\eta}^2 (\lambda - \eta_t)^2}$. Instead of determining the drift of S_t by applying Itô's lemma to $S_t = Y_t \phi_t$ we use the pricing equation instead. Specifically,

$$dR_t - r_t dt = -\frac{dM_t}{M_t} \frac{dS_t}{S_t} = \theta_{\hat{Y},t} \sigma_{\hat{Y}} V_{R,t} + \hat{\theta}_{\eta,t} \sigma_{\eta} \eta_t (\lambda - \eta_t) V_{R,t}.$$

Hence, the instantaneous expected stock market return including dividends is

$$\mu_{R,t} = r_t + \theta_{\hat{Y},t} \sigma_{\hat{Y}} V_{R,t} + \hat{\theta}_{\eta,t} \sigma_{\eta} \eta_t (\lambda - \eta_t) V_{R,t}.$$

□

Proof of Proposition 3. By applying Itô's lemma to the stochastic discount factor (SDF) $M_t = e^{-\rho t} \frac{\mathcal{R}_t}{Y_t}$, we derive the risk-free rate and market prices of risk. The derivation follows the same steps as in the proof of Proposition 1, with the only change being the substitution of $\bar{\mathcal{R}}$ with $\bar{\mathcal{R}}_t$. Therefore, the detailed steps are omitted.

The price-dividend ratio with amplified risk aversion for all $s \leq t < \tau = \infty$ is

$$\phi_t = \mathbb{E}_t \left[\int_t^\infty \frac{M_u Y_u}{M_t Y_t} du \right] = \int_t^\infty e^{-\rho(u-t)} \mathbb{E} \left[\frac{\mathcal{R}_u}{\mathcal{R}_t} \mid \mathcal{R}_t = \mathcal{R}, \tilde{\varepsilon} = \varepsilon \right] du.$$

We have that

$$\mathbb{E}_t \left[\frac{\mathcal{R}_u}{\mathcal{R}_t} \right] = \mathbb{E} \left[\frac{\mathcal{R}_u}{\mathcal{R}_t} \mid \mathcal{R}_t, \tilde{\varepsilon} = \varepsilon \right] = e^{-\kappa_{\mathcal{R}}(u-t)} + \frac{\bar{\mathcal{R}}}{\mathcal{R}_t} (1 - e^{-\kappa_{\mathcal{R}}(u-t)}) + \frac{1}{\mathcal{R}_t} (A_t^1 - A_t^2),$$

with

$$A_t^1 = b\varepsilon\kappa_{\mathcal{R}} e^{-\kappa_{\mathcal{R}}u + \kappa_1 s} \int_t^u e^{(\kappa_{\mathcal{R}} - \kappa_1)a} da \quad \text{and} \quad A_t^2 = b\varepsilon\kappa_{\mathcal{R}} e^{-\kappa_{\mathcal{R}}u + \kappa_2 s} \int_t^u e^{(\kappa_{\mathcal{R}} - \kappa_2)a} da.$$

Suppose that $\kappa_{\mathcal{R}} \neq \kappa_1$ and $\kappa_{\mathcal{R}} \neq \kappa_2$. Then

$$A_t^1 = \frac{b\varepsilon\kappa_{\mathcal{R}}}{\kappa_{\mathcal{R}} - \kappa_1} (e^{-\kappa_1(u-s)} - e^{-\kappa_{\mathcal{R}}(u-t) - \kappa_1(t-s)}), \quad \text{and} \quad A_t^2 = \frac{b\varepsilon\kappa_{\mathcal{R}}}{\kappa_{\mathcal{R}} - \kappa_2} (e^{-\kappa_2(u-s)} - e^{-\kappa_{\mathcal{R}}(u-t) - \kappa_2(t-s)}).$$

The equilibrium price-dividend ratio is then given by

$$\begin{aligned} \phi_t &= \frac{1}{\rho + \kappa_{\mathcal{R}}} + \frac{\bar{\mathcal{R}}}{\mathcal{R}_t} \left(\frac{1}{\rho} - \frac{1}{\rho + \kappa_{\mathcal{R}}} \right) + \frac{b\varepsilon\kappa_{\mathcal{R}}}{\mathcal{R}_t} \left(\frac{e^{-\kappa_1(t-s)}}{(\rho + \kappa_1)(\rho + \kappa_{\mathcal{R}})} - \frac{e^{-\kappa_2(t-s)}}{(\rho + \kappa_2)(\rho + \kappa_{\mathcal{R}})} \right) \\ &= \phi_0 + \phi_{\mathcal{R}} \frac{1}{\mathcal{R}_t} + \phi_{\mathcal{R}}^{amp.RA}(t) \frac{1}{\mathcal{R}_t}, \end{aligned}$$

where $\phi_0 = 1/(\rho + \kappa_{\mathcal{R}})$ and $\phi_{\mathcal{R}} = \bar{\mathcal{R}}\phi_0\kappa_{\mathcal{R}}/\rho$ is as in Proposition 2 and $\phi_{\mathcal{R}}^{amp.RA}(t)$ is given in Equation (26). □

Proof of Proposition 4. Recall that the valuation ratio is

$$\phi_t = \phi_0 + \phi_1(t) \frac{1}{\mathcal{R}_t}, \quad \phi_1(t) = \phi_{\mathcal{R}} + \phi_{\mathcal{R}}^{amp.RA}(t).$$

The dynamics of the valuation ratio ϕ_t are

$$\frac{d\phi_t}{\phi_t} = \frac{1}{\mathcal{R}_t} \frac{d\phi_1(t)/dt}{\phi_t} + \frac{\phi_1(t)}{\phi_t} d\left(\frac{1}{\mathcal{R}_t}\right) = \frac{1}{\mathcal{R}_t} \frac{d\phi_1(t)/dt}{\phi_t} - \frac{\phi_1(t)}{\phi_t} \frac{d\mathcal{R}_t}{\mathcal{R}_t^2} + \frac{\phi_1(t)}{\phi_t} \frac{(d\mathcal{R}_t)^2}{\mathcal{R}_t^3}. \quad (\text{A7})$$

Similarly to the proof of Proposition 2 we determine the stochastic part for the valuation ratio.

$$\frac{d\phi_t}{\phi_t} = \dots dt + \alpha \frac{\phi_1(t)/\mathcal{R}_t}{\phi_t} \left(1 - \frac{\lambda_{\mathcal{R}}}{\mathcal{R}_t}\right) \begin{cases} \sigma_{\hat{Y}} dZ_{\hat{Y},t} + \sigma_{\eta} (\lambda - \eta_t) dZ_{\eta,t} & \text{if } \omega_t = L \\ \sigma_{\hat{Y}} dZ_{\hat{Y},t} & \text{if } \omega_t = H \end{cases} \quad (\text{A8})$$

The equilibrium stock price is $S_t = Y_t \phi_t$ and its instantaneous return including dividends is

$$dR_t \equiv \frac{dS_t + Y_t dt}{S_t} = \mu_{R,t} dt + \sigma_{R,\hat{Y},t} dZ_{\hat{Y},t} + \sigma_{R,\eta,t} dZ_{\eta,t}$$

Suppose $\omega_t = H$, applying Itô's lemma to $S_t = Y_t \phi_t$ leads to

$$\frac{dS_t}{S_t} = \frac{d\hat{Y}_t}{\hat{Y}_t} + \frac{d\phi_t}{\phi_t} + \frac{d\hat{Y}_t}{\hat{Y}_t} \frac{d\phi_t}{\phi_t} = \dots dt + \sigma_{\hat{Y}} dZ_{\hat{Y},t} + \alpha \frac{\phi_1(t)/\mathcal{R}_t}{\phi_t} \left(1 - \frac{\lambda_{\mathcal{R}}}{\mathcal{R}_t}\right) \sigma_{\hat{Y}} dZ_{\hat{Y},t}.$$

Hence, $\sigma_{R,\hat{Y},t} = \sigma_{\hat{Y}} V_{R,t}$ and $\sigma_{R,\eta,t} = 0$ with

$$V_{R,t} = 1 + \alpha \frac{\phi_1(t)/\mathcal{R}_t}{\phi_t} \left(1 - \frac{\lambda_{\mathcal{R}}}{\mathcal{R}_t}\right). \quad (\text{A9})$$

Suppose $\omega_t = L$, applying Itô's lemma to $S_t = Y_t \phi_t$, using Equation (A6) leads to

$$\frac{dS_t}{S_t} = \frac{dY_t}{Y_t} + \frac{d\phi_t}{\phi_t} + \frac{dY_t}{Y_t} \frac{d\phi_t}{\phi_t} = \dots dt + V_{R,t} \sigma_{\hat{Y}} dZ_{\hat{Y},t} + V_{R,t} \sigma_{\eta} (\lambda - \eta_t) dZ_{\eta,t}.$$

Hence, we have that $\sigma_{R,\hat{Y},t} = \sigma_{\hat{Y}}V_{R,t}$ and $\sigma_{R,\eta,t} = V_{R,t}\sigma_{\eta}(\lambda - \eta_t)$. If $\omega_t = H$, then the instantaneous stock market volatility is $\sigma_{R,t} = \sigma_{\hat{Y}}V_{R,t}$. The Brownian shocks $Z_{\hat{Y},t}$ and $Z_{\eta,t}$ are independent and thus the instantaneous stock market volatility if $\omega_t = L$ is $\sigma_{R,t} = V_{R,t}\sqrt{\sigma_{\hat{Y}}^2 + \sigma_{\eta}^2(\lambda - \eta_t)^2}$. Instead of determining the drift of S_t by applying Itô's lemma to $S_t = Y_t\phi_t$, we use the pricing equation instead. Specifically,

$$dR_t - r_t dt = -\frac{dM_t}{M_t} \frac{dS_t}{S_t} = \theta_{\hat{Y},t}\sigma_{\hat{Y}}V_{R,t} + \hat{\theta}_{\eta,t}\sigma_{\eta}\eta_t(\lambda - \eta_t)V_{R,t}.$$

Hence, the instantaneous expected stock market return including dividends is

$$\mu_{R,t} = r_t + \theta_{\hat{Y},t}\sigma_{\hat{Y}}V_{R,t} + \hat{\theta}_{\eta,t}\sigma_{\eta}\eta_t(\lambda - \eta_t)V_{R,t}.$$

Substituting the market prices of risk and volatility exposures, followed by some algebraic manipulation, completes the proof. \square

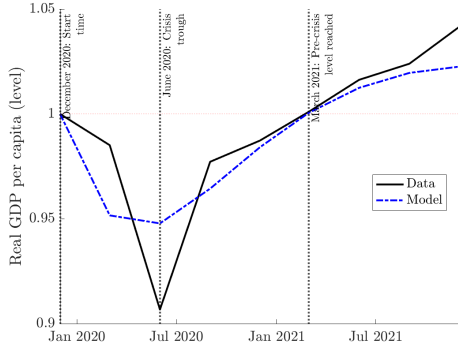
Appendix B. Fitting output dynamics during other crises

Here, we replicate the procedure outlined in Section V to fit output data from NBER crisis periods since 1947. Specifically, we minimize the error function from equation (29) using observed output data for each crisis episode. The weight parameter w is set to 0.9. Consistent with the estimation for the GFC, we target the average unconditional crisis-to-non-crisis volatility ratio of 1.8911. To achieve this, we simulate 10,000 paths of quarterly observations, ensuring that the length of each simulated time series matches the observed duration of each recession. Using the parameters from Table II, we estimate the remaining five crisis-specific parameters $\theta = (\kappa_1, \kappa_2, \kappa_{\eta}, \sigma_{\eta}, \varepsilon)$.

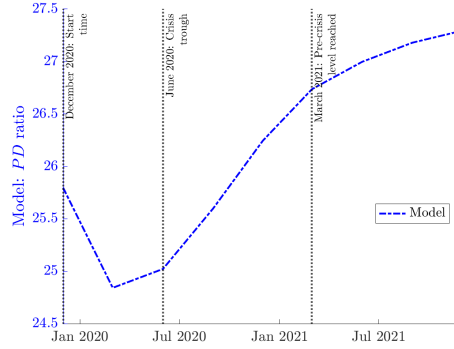
Below, we present the matched output and the model-implied asset-pricing moments for each crisis estimation (in blue), along with the corresponding estimated values $\hat{\theta}$. When data

is available, we also include the empirical counterparts of the implied asset-pricing moments (in black).

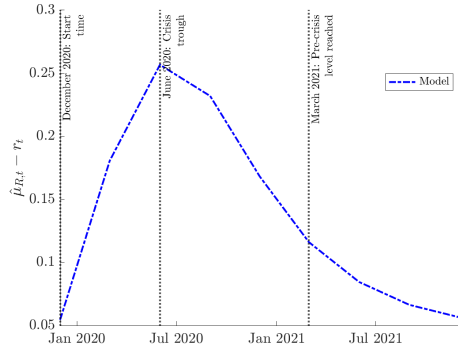
COVID-19 Recession



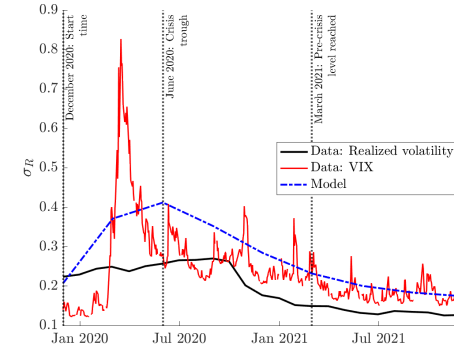
(a) Output level



(b) Price-dividend ratio



(c) Risk premium



(d) Return volatility

Figure B.1. This figure compares the mean simulated model predictions (blue dashed-dotted lines) with empirical observations when data is available. Panel (a) shows real GDP per capita (black solid line) alongside model predictions. Panel (b) presents the model-implied equity risk premia. Panel (c) reports the price-dividend ratio. Panel (d) compares model predictions with monthly realized volatility (black solid line) and the VIX (red line). The model predictions are generated using $b = 300$, with the estimated parameters provided below.

Parameter θ_i	Estimated Value
κ_1	4.3399
κ_2	6.1888
κ_η	1.5664
σ_η	0.5856
ε	1.0830

Early 1990s Recession

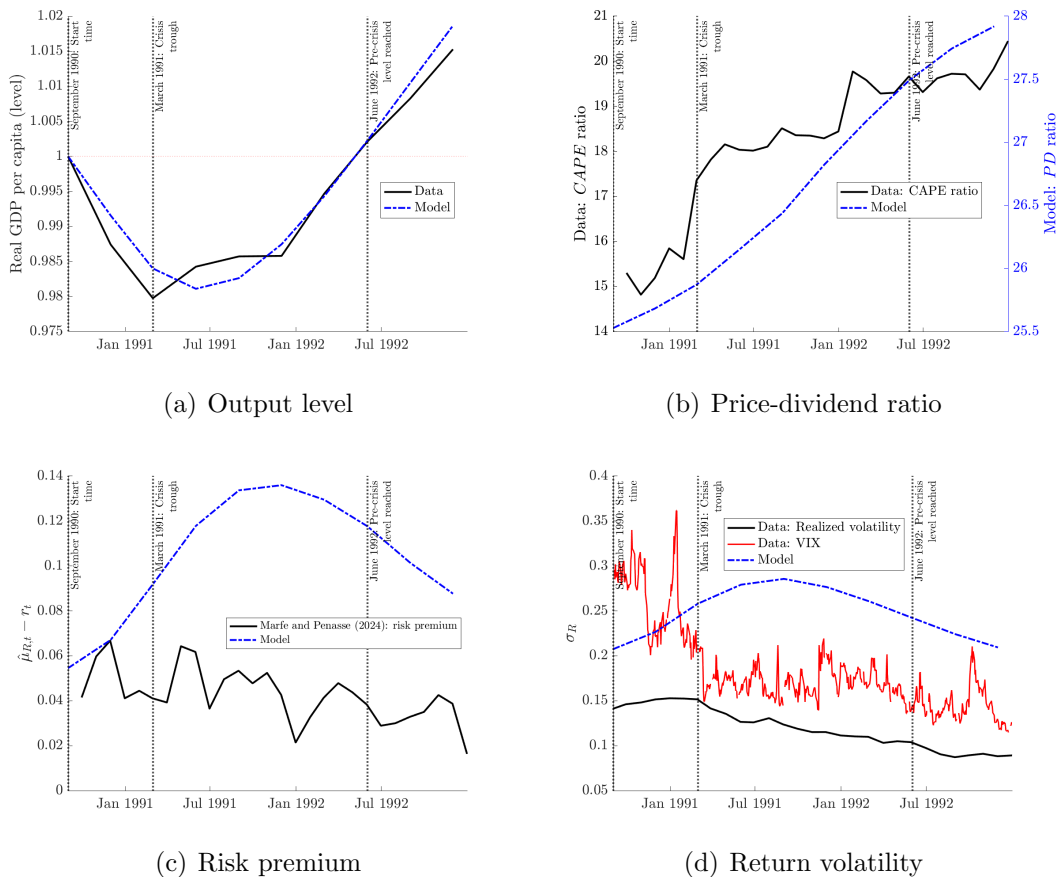


Figure B.2. This figure compares the mean simulated model predictions (blue dashed-dotted lines) with empirical observations when data is available. Panel (a) shows real GDP per capita (black solid line) alongside model predictions. Panel (b) compares the model-implied equity risk premia with the Marfè and Pénasse (2024) index. Panel (c) reports the CAPE ratio (black solid line). Panel (d) compares model predictions with monthly realized volatility (black solid line) and the VIX (red solid line). The model predictions are generated using $b = 100$, with the estimated parameters provided below.

Parameter	Estimated Value
κ_1	0.6857
κ_2	2.2501
κ_η	1.9471
σ_η	0.6176
ε	0.1002

Recession of 1981-82

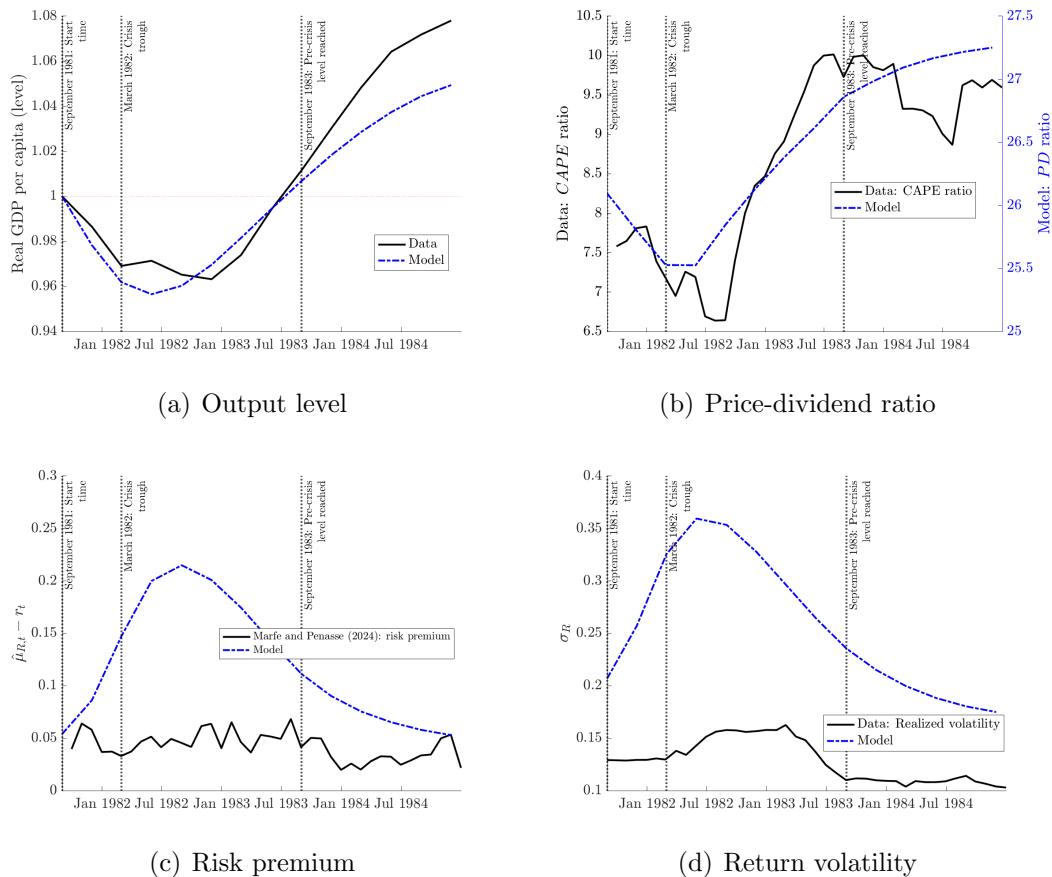
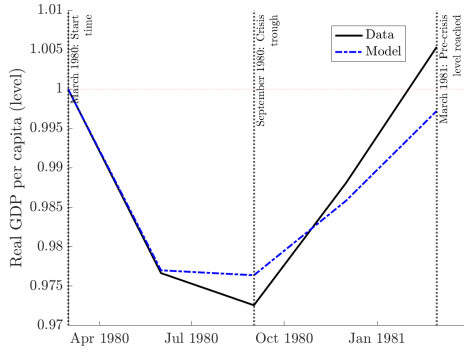


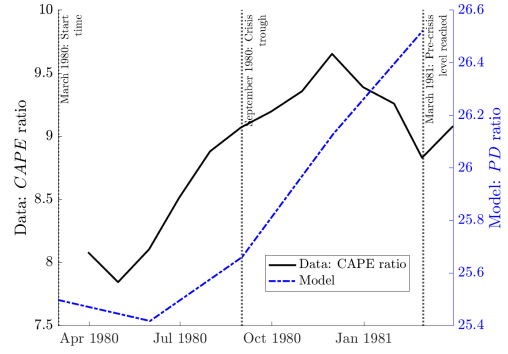
Figure B.3. This figure compares the mean simulated model predictions (blue dashed-dotted lines) with empirical observations when data is available. Panel (a) shows real GDP per capita (black solid line) alongside model predictions. Panel (b) compares the model-implied equity risk premia with the Marfè and Pénasse (2024) index. Panel (c) reports the CAPE ratio (black solid line). Panel (d) compares model predictions with monthly realized volatility (black solid line). The model predictions are generated using $b = 300$, with the estimated parameters provided below.

Parameter	Estimated Value
κ_1	1.5621
κ_2	2.8040
κ_η	1.5822
σ_η	0.2542
ε	0.3466

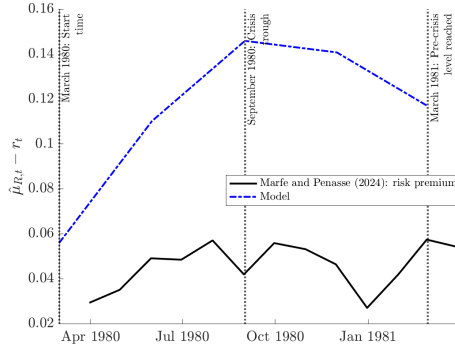
Recession of 1980



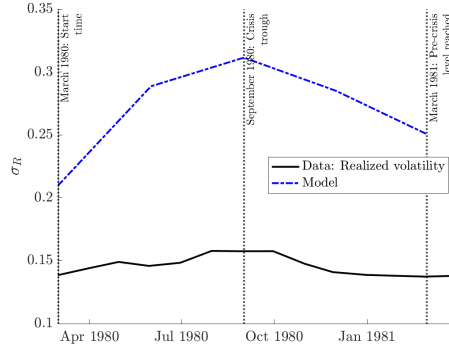
(a) Output level



(b) Price-dividend ratio



(c) Risk premium



(d) Return volatility

Figure B.4. This figure compares the mean simulated model predictions (blue dashed-dotted lines) with empirical observations when data is available. Panel (a) shows real GDP per capita (black solid line) alongside model predictions. Panel (b) compares the model-implied equity risk premia with the Marfè and Pénasse (2024) index. Panel (c) reports the CAPE ratio (black solid line). Panel (d) compares model predictions with monthly realized volatility (black solid line). The model predictions are generated using $b = 200$, with the estimated parameters provided below.

Parameter	Estimated Value
κ_1	1.9933
κ_2	10.0000
κ_η	1.9878
σ_η	0.6979
ε	0.1064

Recession of 1973-75

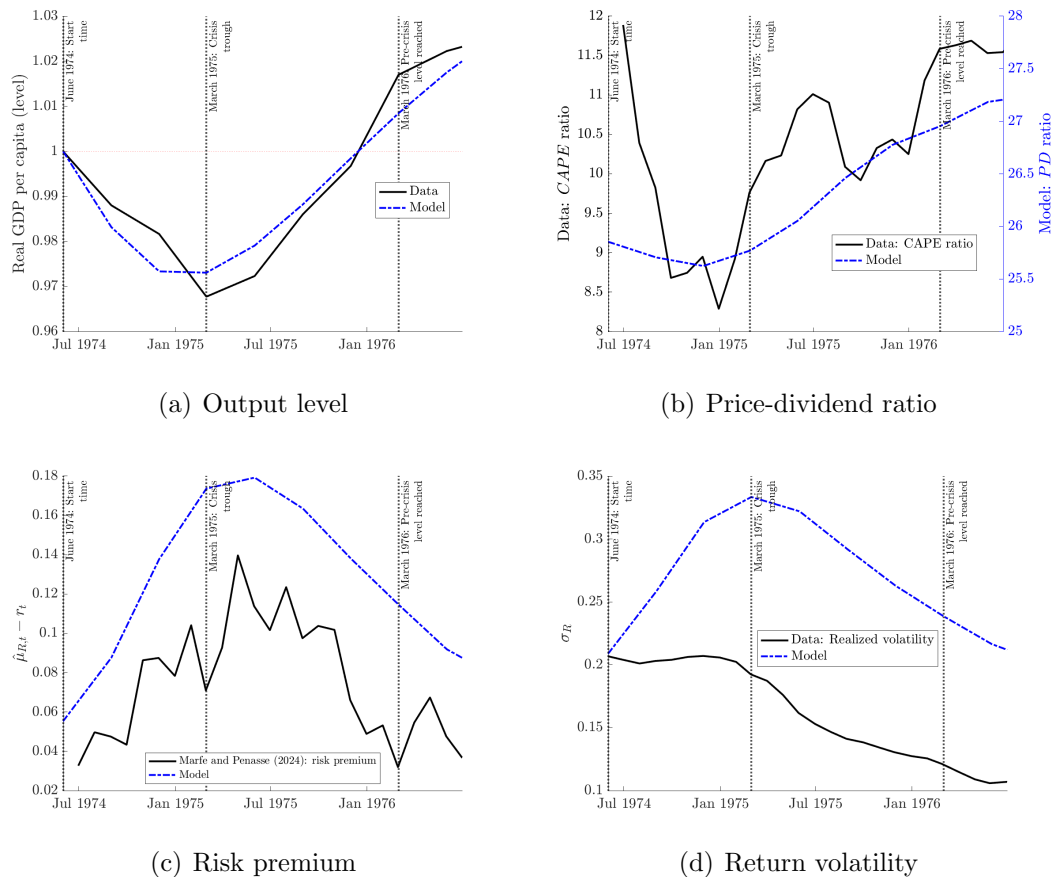


Figure B.5. This figure compares the mean simulated model predictions (blue dashed-dotted lines) with empirical observations when data is available. Panel (a) shows real GDP per capita (black solid line) alongside model predictions. Panel (b) compares the model-implied equity risk premia with the Marfe and Pénasse (2024) index. Panel (c) reports the CAPE ratio (black solid line). Panel (d) compares model predictions with monthly realized volatility (black solid line). The model predictions are generated using $b = 300$, with the estimated parameters provided below.

Parameter	Estimated Value
κ_1	0.9943
κ_2	3.8906
κ_η	1.9613
σ_η	0.6405
ε	0.1105

Recession of 1969-70

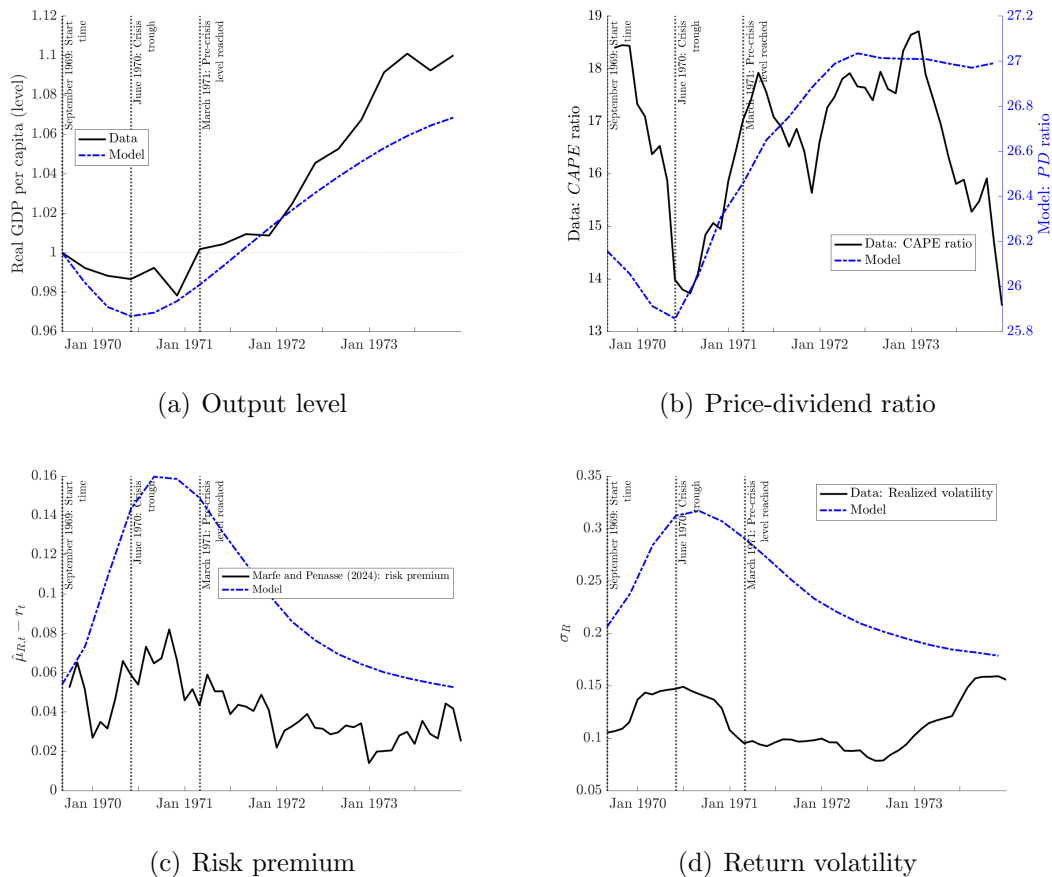


Figure B.6. This figure compares the mean simulated model predictions (blue dashed-dotted lines) with empirical observations when data is available. Panel (a) shows real GDP per capita (black solid line) alongside model predictions. Panel (b) compares the model-implied equity risk premia with the Marfè and Pénasse (2024) index. Panel (c) reports the CAPE ratio (black solid line). Panel (d) compares model predictions with monthly realized volatility (black solid line). The model predictions are generated using $b = 300$, with the estimated parameters provided below.

Parameter	Estimated Value
κ_1	0.6230
κ_2	3.2064
κ_η	1.8582
σ_η	0.5190
ε	0.1065

Recession of 1958

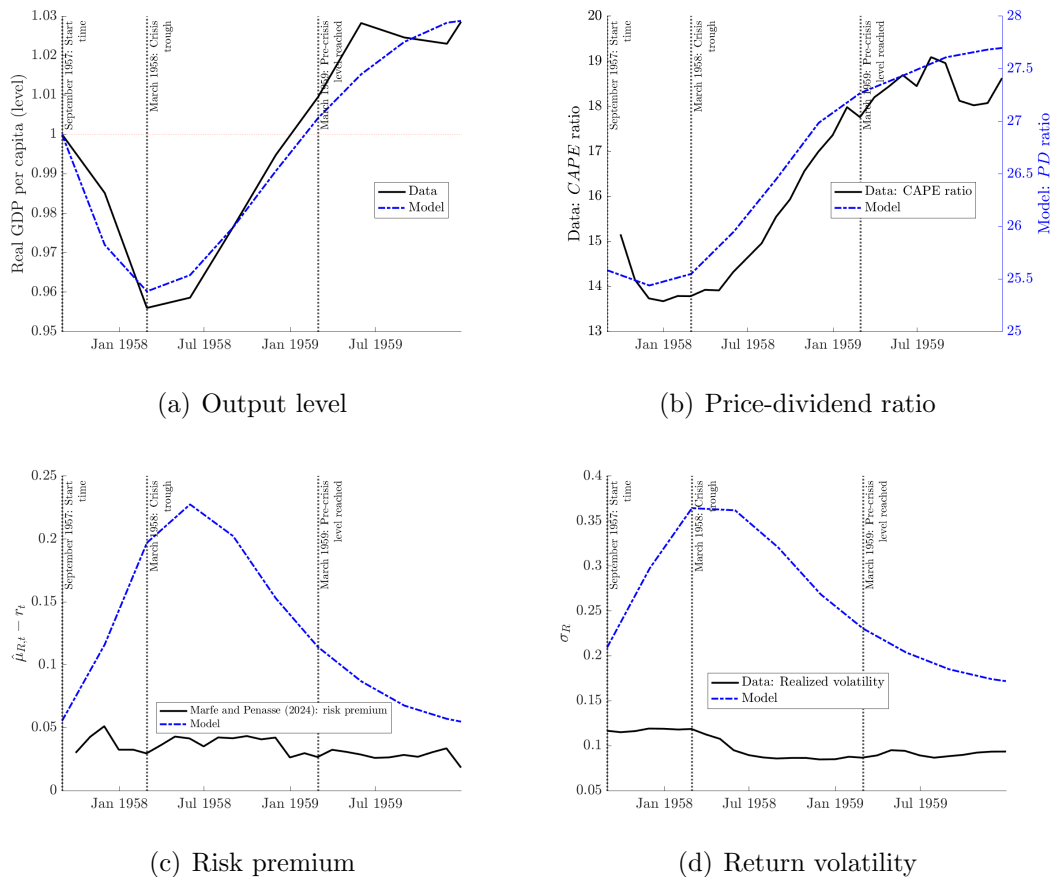


Figure B.7. This figure compares the mean simulated model predictions (blue dashed-dotted lines) with empirical observations when data is available. Panel (a) shows real GDP per capita (black solid line) alongside model predictions. Panel (b) compares the model-implied equity risk premia with the Marfè and Pénasse (2024) index. Panel (c) reports the CAPE ratio (black solid line). Panel (d) compares model predictions with monthly realized volatility (black solid line). The model predictions are generated using $b = 200$, with the estimated parameters provided below.

Parameter	Estimated Value
κ_1	1.8035
κ_2	4.0918
κ_η	1.9886
σ_η	0.6403
ε	0.2377

Recession of 1953

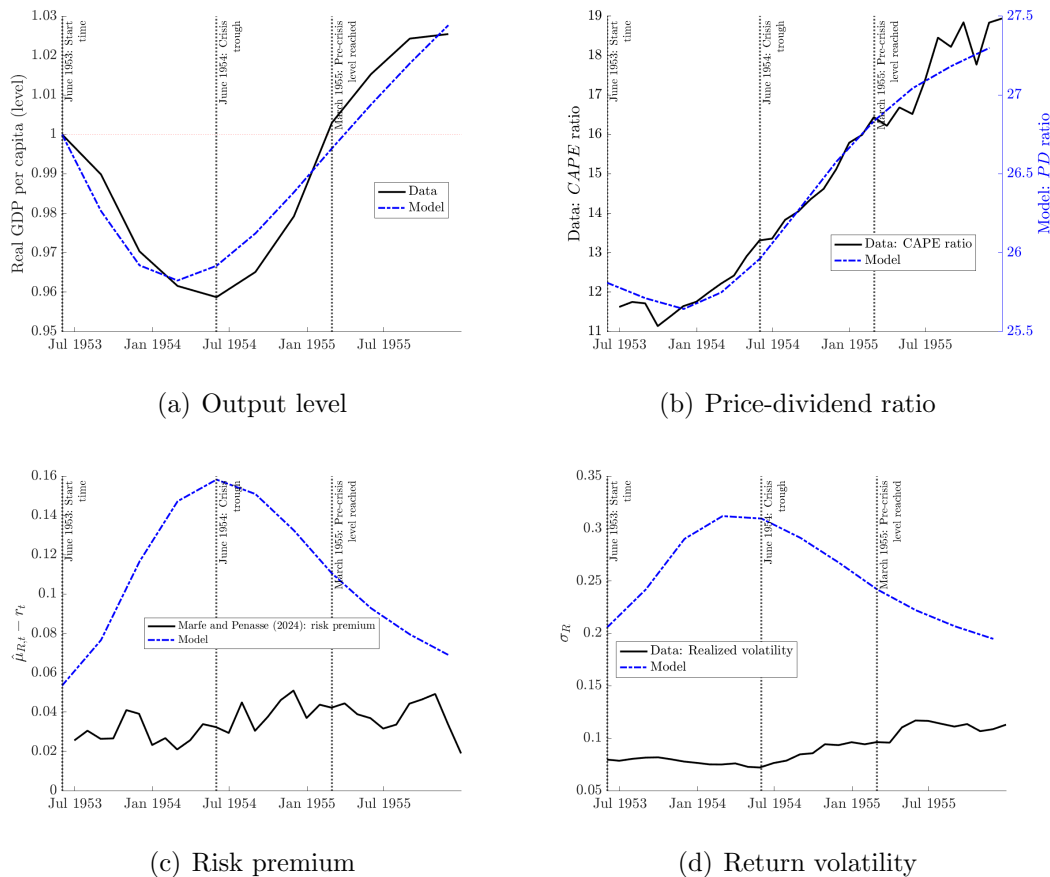


Figure B.8. This figure compares the mean simulated model predictions (blue dashed-dotted lines) with empirical observations when data is available. Panel (a) shows real GDP per capita (black solid line) alongside model predictions. Panel (b) compares the model-implied equity risk premia with the Marfè and Pénasse (2024) index. Panel (c) reports the CAPE ratio (black solid line). Panel (d) compares model predictions with monthly realized volatility (black solid line). The model predictions are generated using $b = 500$, with the estimated parameters provided below.

Parameter	Estimated Value
κ_1	0.9129
κ_2	3.9515
κ_η	1.6304
σ_η	0.5015
ε	0.1404

Recession of 1949

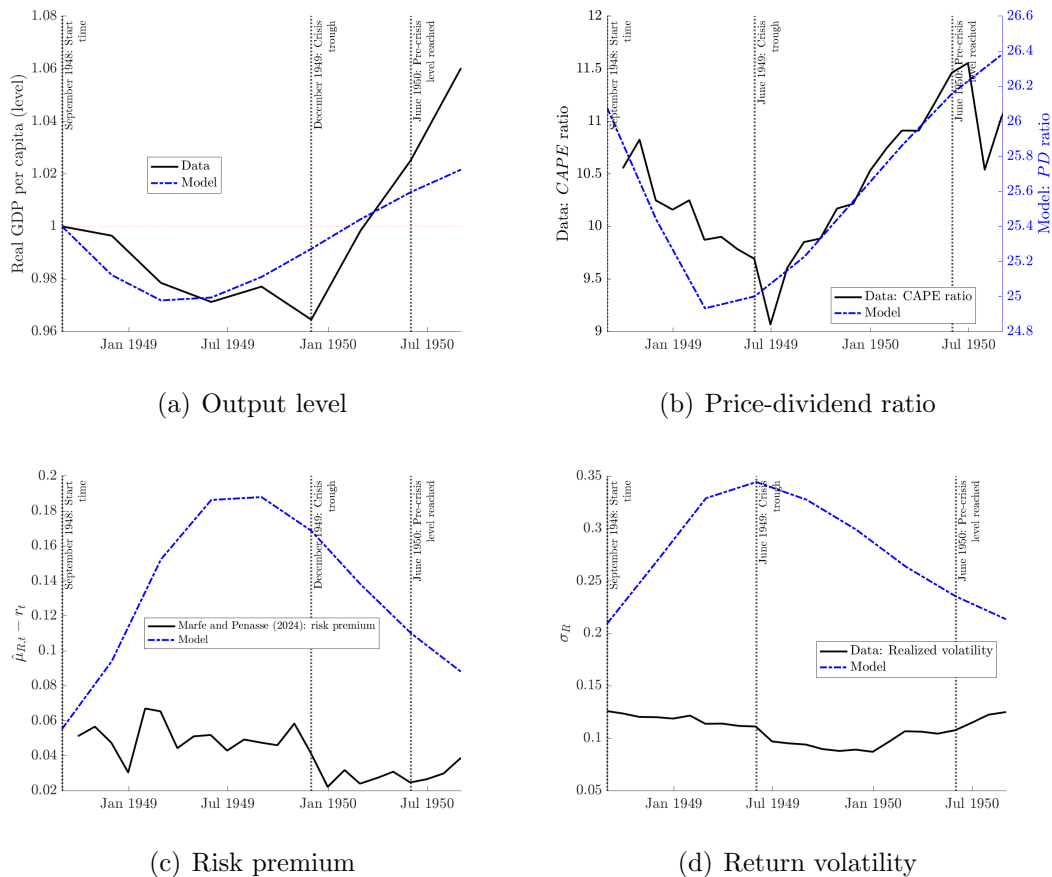


Figure B.9. This figure compares the mean simulated model predictions (blue dashed-dotted lines) with empirical observations when data is available. Panel (a) shows real GDP per capita (black solid line) alongside model predictions. Panel (b) compares the model-implied equity risk premia with the Marfè and Pénasse (2024) index. Panel (c) reports the CAPE ratio (black solid line). Panel (d) compares model predictions with monthly realized volatility (black solid line). The model predictions are generated using $b = 500$, with the estimated parameters provided below.

Parameter	Estimated Value
κ_1	1.6465
κ_2	4.3864
κ_η	1.5272
σ_η	0.6201
ε	0.1860